European Journal of Life Sciences

Volume: 1 • Issue: 2 • August 2022 • ISSN: 2822-5333

ANADOLU UNIVERSITY
INSTITUTE OF HEALTH SCIENCES

ANADOLU UNIVERSITY
INSTITUTE OF HEALTH SCIENCES

European Journal of Life Sciences

Volume: 1 • Issue: 2 • August 2022

ISSN: 2822-5333

European Journal of Life Sciences

Owner of the Journal on behalf of Anadolu University
Prof. Dr. Fuat Erdal

Editor in Chief
Prof. Dr. Gülşen Akalın Çiftçi

Editors
Prof. Dr. Yavuz Bülent Köse
Prof. Dr. Gökalp İşcan
Assoc. Prof. Dr. Mustafa Sinan Kaynak
Assoc. Prof. Dr. Hale Gamze Ağalar

Publication Type
International peer-reviewed journal

Publication Frequency
Triannually

Language
English

Website
https://dergipark.org.tr/ejls

Publisher
Anadolu University Institute of Health Sciences

Publisher Address
Anadolu University, Institute of Health Sciences, Yunus Emre Campus, 26470 Tepebaşı/Eskişehir.
Phone: +90 222 320 76 51
E-mail: sagens@anadolu.edu.tr
Web: https://sbe.anadolu.edu.tr/en

Publishing Services
Akdema Informatics, Publishing, and Consultancy Trade LLC
Address: Kızılay Mahallesi, Gazi Mustafa Kemal Bulvarı No: 23/8, 06420 Çankaya/Ankara
E-mail: bilgi@akdema.com
Phone: +90 533 166 80 80
Web site: www.akdema.com

European Journal of Life Sciences

Editorial Board

European Journal of Life Sciences

Contents

ANADOLU UNIVERSITY
INSTITUTE OF HEALTH SCIENCES

European Journal of Life Sciences 2022; 1: 35-45

Research Article

Morpho-anatomical and palynological properties of endemic *Astragalus tmoleus* var. *bounacanthus* (Fabaceae)*

Ayla Kaya[1]

[1]Anadolu University, Faculty of Pharmacy, Department of Pharmaceutical Botany, Eskişehir, Turkey.

✉ Ayla Kaya
aykaya@anadolu.edu.tr

https://doi.org/10.55971/EJLS.1147134

Received: 22.07.2022
Accepted: 13.10.2022
Available online: 21.10.2022

*The article was presented as a poster presentation at the XI. International Ethnobotanic Symposium held in Antalya-TURKEY on 2-5 November 2013.

ABSTRACT

Astragalus tmoleus Boiss. var. *bounacanthus* (Boiss.) Chamberlain is a member of the *Pterophorus* Bunge section of the Fabaceae family and consists of the spiny cushion-forming shrub. In this study, morphological, anatomical and pollen properties of the plant, an endemic species for Turkey, have been investigated in detail. Morphological characters such as the shape of paripinnate leaves, stipules and bracts, the flower number in the inflorescence, the stenonychioid type of standard and the reniform type of seed can be helpful to distinguish *A. tmoleus* var. *bounacanthus*. The stem, leaf and rachis characteristics of the plant were examined in anatomical studies. There is a secondary growth in stem anatomy. The number of vascular bundles is 15-18 in a circle. The shape of the transversal section of the rachis is polygonal or almost orbicular. The sclerenchyma tissue is located on the vascular bundles in the rachis. *A. tmoleus* var. *bounacanthus* has equifasial leaves. The stomata type is anomocytic and occurs on both leaflet epidermises. The pollen grains of *A. tmoleus* var. *bounacanthus* have tricolpate aperture and they are subprolate-shaped. While the pollen exine sculpturing is microreticulate, the seed surface sculpturing is a prominent undulate-ridged pattern formed by irregular cells. Scanning electron microscopy (SEM) is used to determine pollen and seed morphology.

Keywords: Anatomy, *Astragalus tmoleus* var. *bounacanthus*, Morphology, Pollen, Seed

1. INTRODUCTION

The genus *Astragalus* L. (Fabaceae) which is one of the largest genera of vascular plants in the world, is distributed in semi-arid steppe regions. It is represented by c. 3000 species and more than 250 sections. Turkey is one of the most important centers of distribution of the genus *Astragalus* and it is represented by 476 taxa, 64 sections. It has high endemism rates, with a value of 51% in Turkey [1-4].

Astragalus species are economically important because most of them produce the valuable tragacanth gum and selenium. Tragacanth gum is recorded Tragacantha or Gummi Tragacantha in the name codex and pharmacopoeias [5]. The genus *Astragalus* is also ecologically important because most of the provide pillows and play a very important role in the prevention of erosion. However, they are consumed in mountainous and rural areas as firewood and animal feed [6]. The roots of some *Astragalus* species represent very old and well-known drugs in traditional medicine for the treatment of nephritis, diabetes, and uterine cancer and as antiperspirant, diuretic, and tonic. In Turkish folk medicine, the aqueous extracts of various *Astragalus* species are used to treat leukemia as well as for wound healing [7].

A. tmoleus Boiss. is an element of the Mediterranean phytogeographical mainly distributed on stony slopes of the southwest and central Anatolia region. It is a member of the section *Pterophorus* and it grows on stone slopes of central and south-west Anatolia in 800-2000 m [1]. *A. tmoleus* is represented by two varieties (var. *tmoleus* and var. *bounacanthus* (Boiss.) Chamberlain in the Flora of Turkey. Both of varieties are used by chewing the resin for toothache, abdominal pain in cattle and small ruminants [8]. A previous study by Pirdal et al. (1991) reported the morphology, anatomy and ecology of *A. tmoleus* var. *tmoleus* [9].

In this study, morphological, anatomical, palynological and seed surface properties of endemic *A. tmoleus* var. *bounacanthus* were investigated in detail for the first time.

2. MATERIALS AND METHODS

2.1. Plant Material

A. tmoleus var. *bounacanthus* was collected during the flowering and fruiting periods (July-September, 2011) from Eskişehir (Karacaşehir-Eşenkara köyü, 39º 42’ 42’’K ve 30º 25’ 40’’D) province of Turkey. Voucher specimens are deposited in the Herbarium of the Faculty of Pharmacy of Anadolu University in Eskisehir (ESSE 14578), Turkey.

2.2. Microscope Studies

Macromorphological observations (20 samples) were carried out under a binocular stereomicroscope, Olympus SZX12 with a drawing tube. Live material was stored in 70% ethanol for anatomical studies. All sections were made manually and taken from the middle regions of the plant. All sections (60 sections) were embedded in glycerin-gelatine and mounted on microscope slides with Canadian Balsam. Olympus BX51 binocular light microscope and camera were used. Photographs were taken. For the SEM study, the pollen (more than 50 pollen grains) and seed specimens (10 specimens) were mounted onto SEM stubs using double-sided adhesive tape and coated with gold. Photographs were taken with the electron microscope (Zeiss EVO 50).

3. RESULTS

3.1. Morphology

Astragalus tmoleus var. *bounacanthus* is a lax cushion-forming shrub, 10-32 cm. Leaf rachis is 1.9-5 cm, spiny, straight or slightly incurved and haired in lower parts. Leaflets are in (3-) 4-6 (-7) pairs,

Figure 1. *A. tmoleus* Boiss. var. *bounacanthus* (Boiss.) Chamberlain in natural

5-13 x 2.5-5 mm, elliptic, spine-tipped, densely adpressed simple pilose-tomentolleus, cuneate in the base. Stipules are 9-14 x 4-7 mm, ± ovate-lanceolate, tomentellous. Flowers are sessile and they are found in 2-3 per leaf axil. The inflorescence is globose to cylindrical, 2.3-3 cm in diameter and 20-40 flowered. Bracts are ovate-lanceolate, orbicular, bilobed and 8-12 x 5-8 mm and tomentellous. Bracteoles are 7-12 x 1.5-3(-4) mm, linear, densely white pilose, resembling the calyx lobes. The calyx is 10-15 mm,

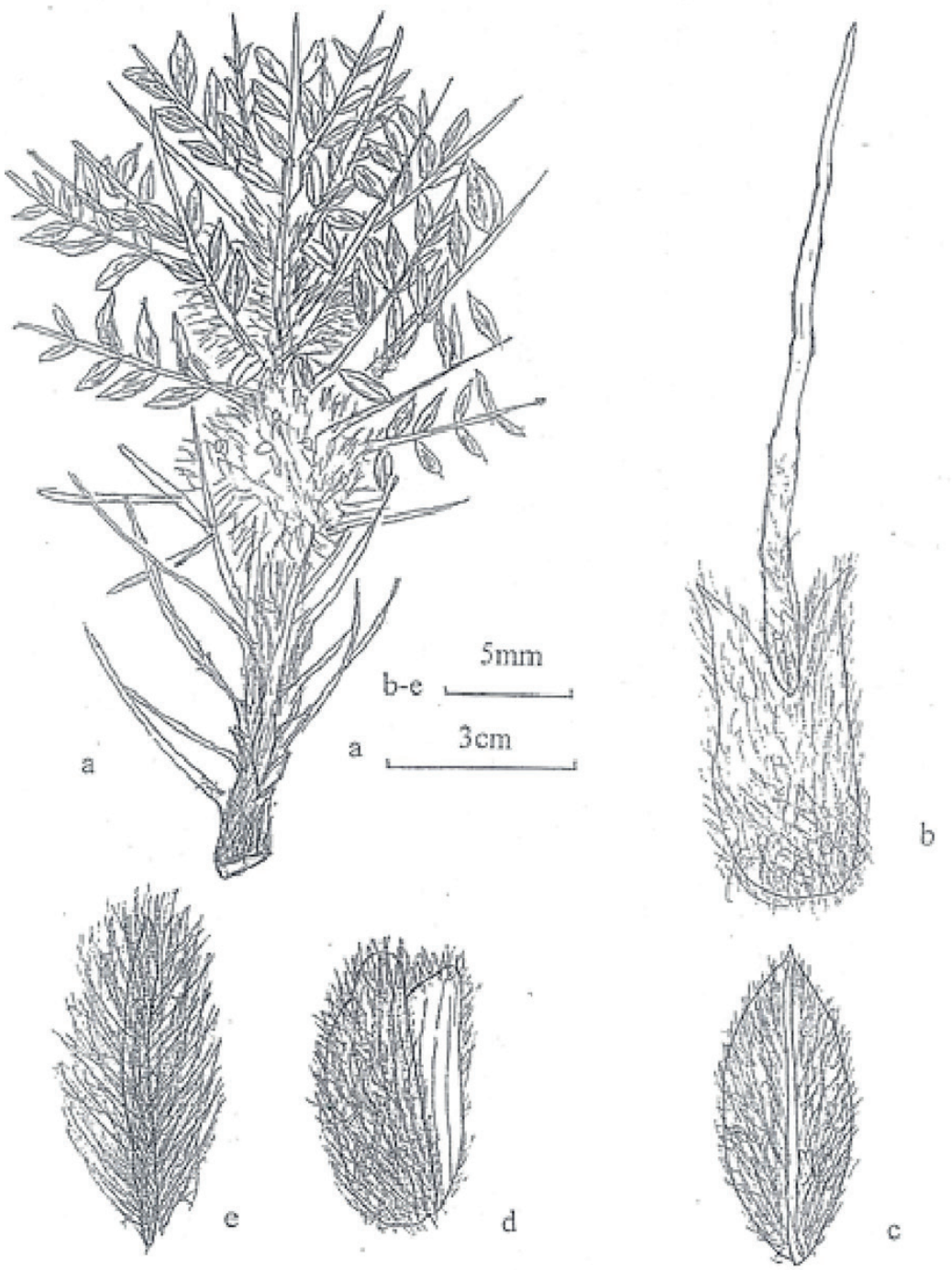

Figure 2. *A. tmoleus* var. *bounacanthus* a. plant b. stipul, c. leaflet, d. bract, e. bracteol

densely white pilose to villous. The lobes of calyx are divided to the base by apparently forming a 2-4 mm tube. Corolla is rosa-pink. The standard is stenonychioid type, 12-18.5 mm, spathulate, obtuse-rotundate in the apex. The wings are 12-18 mm, oblong-triangular in the above and obtuse in the apex. The keels are 12-17 mm, falcate and lobed. The stamen is 11-18 mm, diadelphous. The ovary is 4-6 x 1.8-2.5 mm, ± elliptic, densely long and white-haired. Legumens are 5-7 x 2-5 mm, ovate, densely

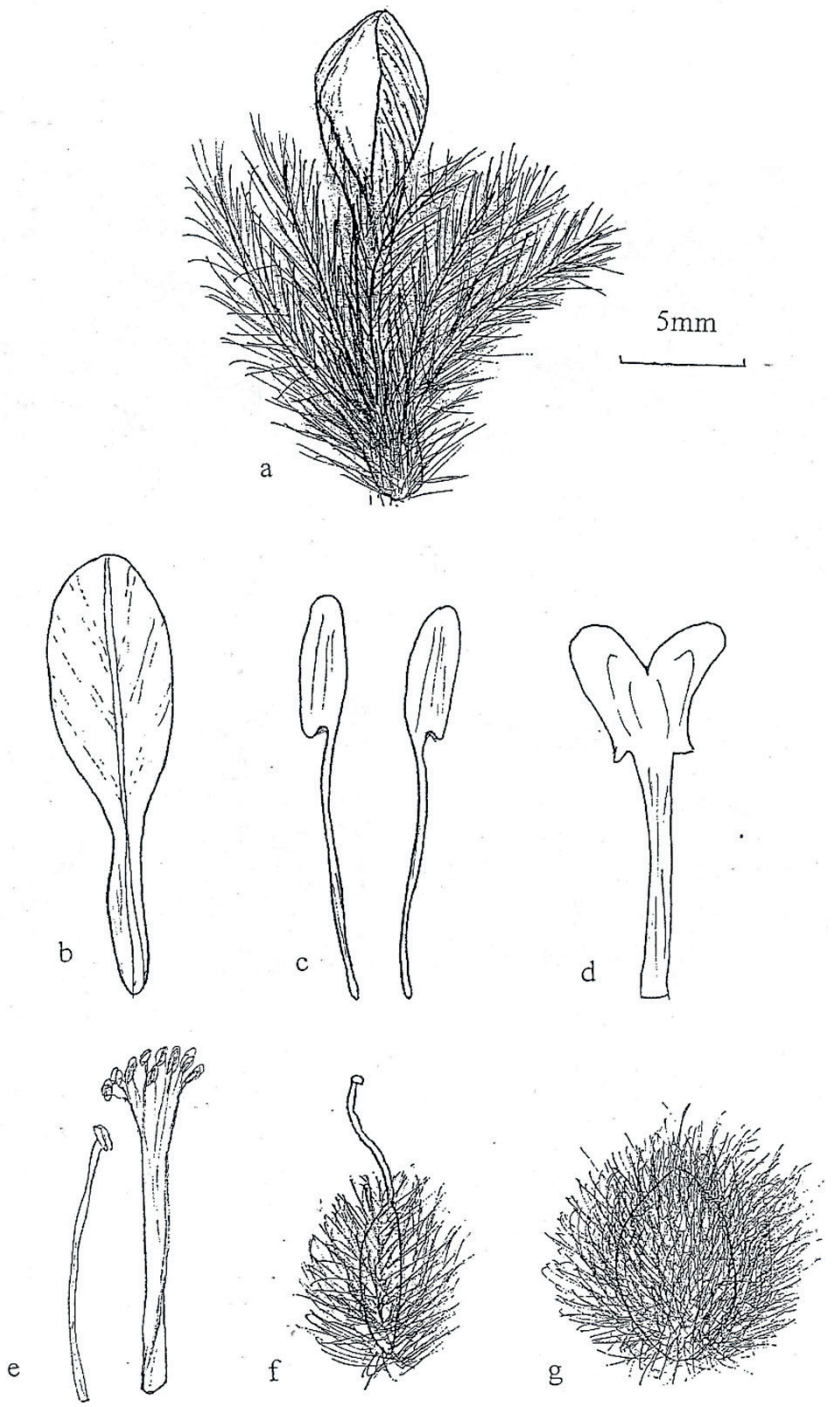

Figure 3. *A. tmoleus* var. *bounacanthus* a. flower, b. standard c. wings d. keel e. diadelphous stamens f. ovarium g. fruit

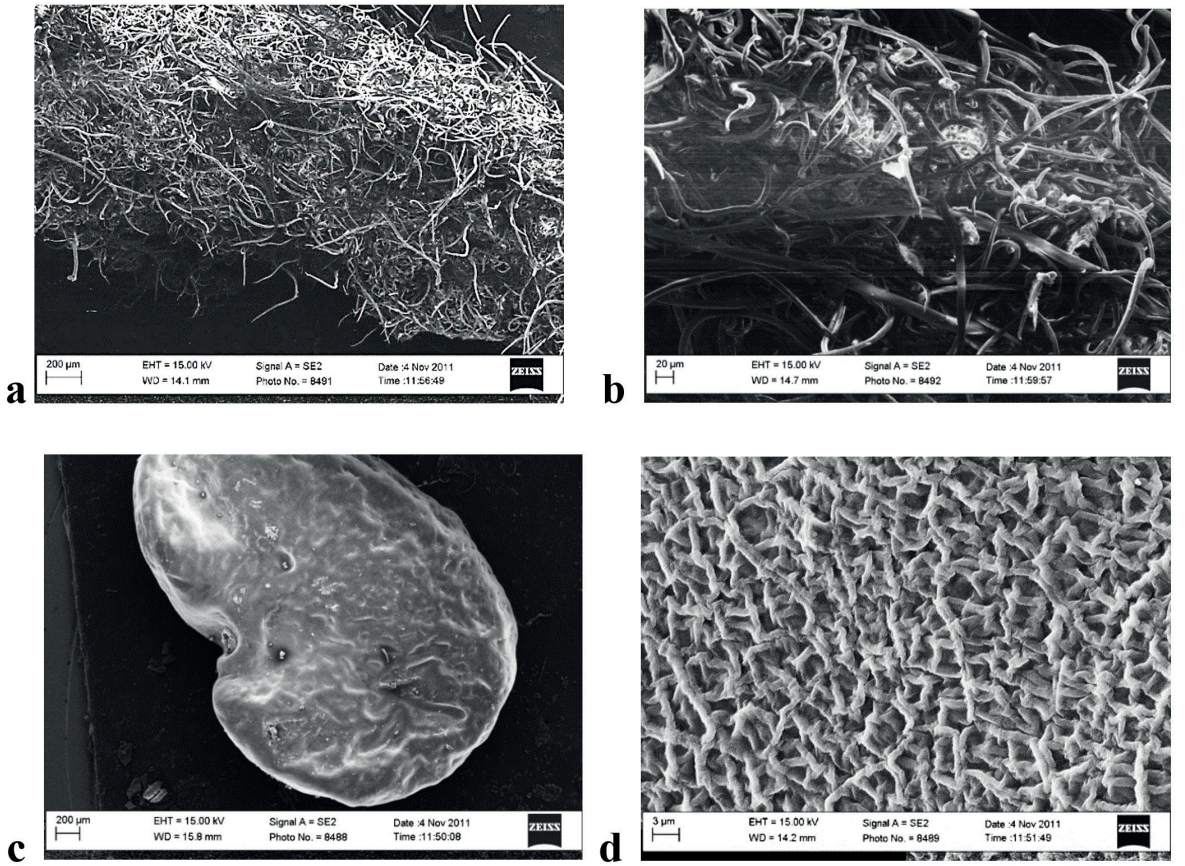

Figure 4. a-b Leaflet upper surface view; c-d Seed and seed surface of *A. tmoleus* var. *bounacanthus* at SEM

long and white-haired. The seeds are (2-) 2.5-3.8 x 1.5-2.5 mm, yellowish-brown and reniforme shaped. The seed surface has a prominent undulate-ridged pattern formed by irregular cells (Figures 1-4).

3.2. Pollen Morphology

The pollen grains are radially symmetrical, isopolar, and have a tricolporate aperture. Polar axis 23.8-34 µm, equatorial axis 17.7-29.3 µm. P/E: 1.16-1.34 µm. The shape of pollen grains is subprolate. Colpi is narrow and long. Clg (13.4-) 18.5–25 µm, Clt (0.2-) 0.4- 0.6 (-1) µm. Exine sculpturing is microreticulate (Figure 5).

3.3. Anatomy

3.3.1. Stem

Transverse sections taken from the middle part of the stem were observed as follows.

The epidermis is composed of a single layer of almost small, square arranged cells. The upper surface is covered with a thick cuticle. Covering trichomes consists of the non-glandular type which is simple, dense and long. The collenchyma tissue is located under the epidermis and occurs from 6-8 layered. The primary cortex is composed of parenchyma cells, 7-15 layered in between the collenchyma and vascular bundle. The shape of these cells is oval-rectangular and they include starch. The secondary cortex is composed of sclerenchyma cells, which are located on the phloem tissue of vascular bundles. The number of vascular bundles is 15-18 in a circle. However, 3-4 vascular bundles are also present in between parenchyma and collenchyma cells. A group of 2-3 stone cells is located in between sclerenchyma and phloem. The shape of phloem cells is irregular-polygonal. The cambium is 4-7-layered, with flattened cells and thin walls. There are secondary xylem under the cambium and primary xylem faces

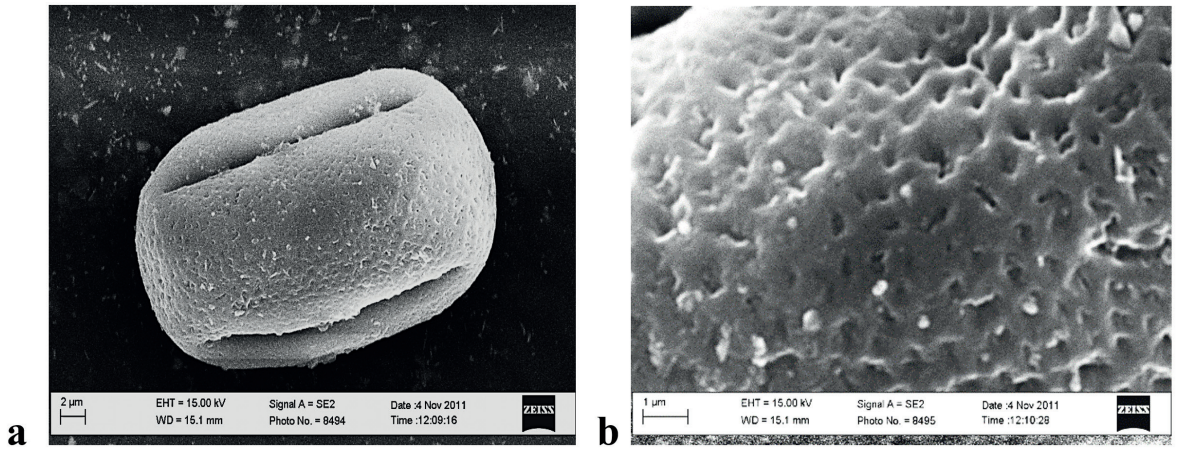

Figure 5. SEM of pollen. a. general view b. ornamentation

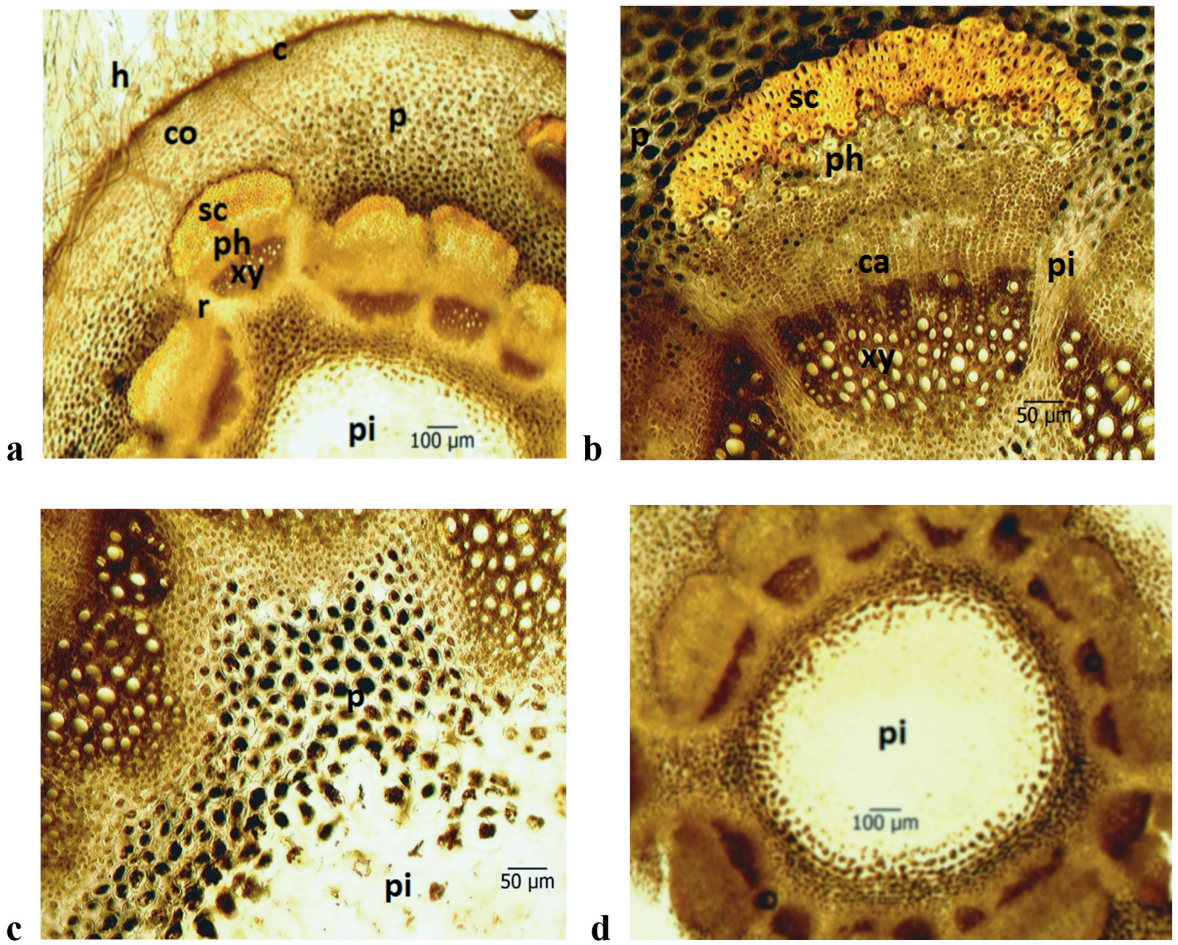

Figure 6. Transverse section of stem. a-general view b-vascular bundle c-d pith; cu-cutikula, co-collenchyma ph-phloem ca-cambium xy-xylem p-parenchyma pi-pith r-ray sc-sclerenchyma h-hair

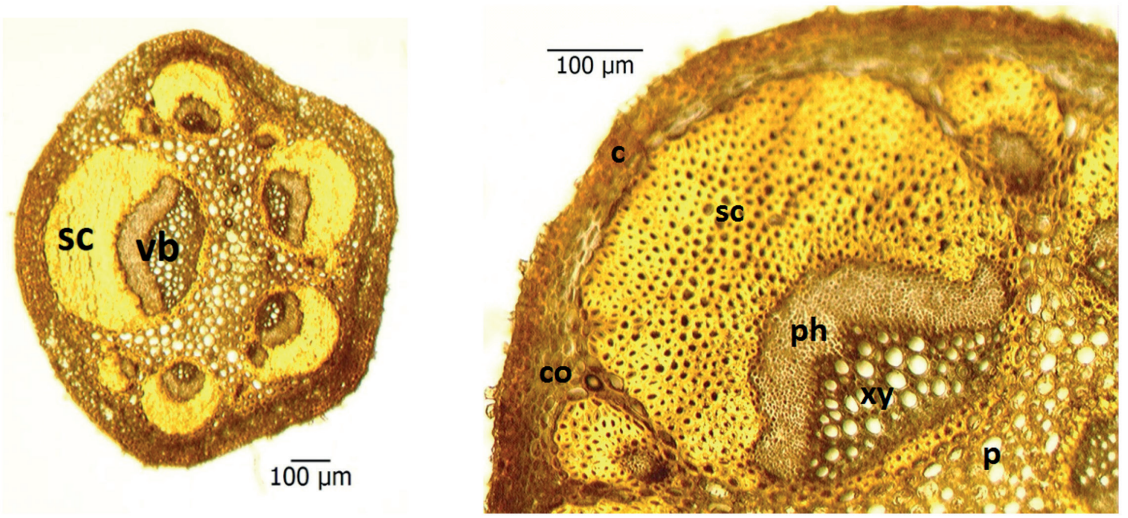

Figure 7. Transverse section of rachis. a-general view b-vascular bundle; co-collenchyma sc-scleranchyma p- parenchyma ph-phloem vb-vascular bundle xy-xylem

toward the pith. Rays are 3-6 (10) layered. The pith consists of large parenchyma cells including abundant starch. After a few layered parenchyma cells, they are rented in the middle stems and large tragacanth spaces in the pith section are occurred (Figure 6).

3.3.2. Rachis

The shape of the transversal section of the rachis is polygonal or almost orbicular. The uppermost of the rachis is a thick cuticle layer and there is an epidermis with one-layered cells under the cuticle. The collenchyma tissue is located under the epidermis and it consists of 3-5-layered and transversally oval-rectangular-shaped cells. The vascular bundles are located one big and 8-14 small at the top and lateral ways of the section after the collenchyma. The vascular bundles are surrounded by broadly and multilayers scleranchymatic cells on the phloem while the sclerenchyma cells are several layers under the xylem. They are polygonal shaped. The vascular bundles are arranged as phloem on the outside and xylem on the inside. The vascular bundles with together sclerenchyma tissue are almost rounded shaped. Pith is composed of parenchymatic cells with a thick wall and it covers a narrow area (Figure 7).

3.3.3. Leaflet

The upper and lower epidermises consist of uniseriate oval and rectangular cells in the transverse section. The upper walls are thicker than the lower and lateral walls. Both epidermises are covered with a thick cuticle and included covering long trichomes. The stomata type is anomocytic and occurs on both leaflet epidermises. The leaflets are the equifacial type which consists of 2 layers palisade parenchyma cells, on the adaxial and abaxial surfaces of the leaflets. The spongy tissue with a row of flattened cells or often indistinct. The midrib region is protruding and bigger than the others. There is also an 8-12 small vascular bundle in lateral regions. The vascular bundles are of the collateral type and surrounded by a parenchymatic bundle sheath. A group of scleranchymatic cells is found below the phloem and they are thick-walled and polygonal shaped. The xylem occupies a narrow area and it faces toward the adaxial epidermis and is surrounded by the phloem. The phloem is between sclerenchyma tissue and xylem and it faces towards the abaxial epidermis. The collenchyma cells are located in between the lower epidermis and bundle sheath while the palisade parenchyma is located in between the upper epidermis and bundle sheath (Figure 8).

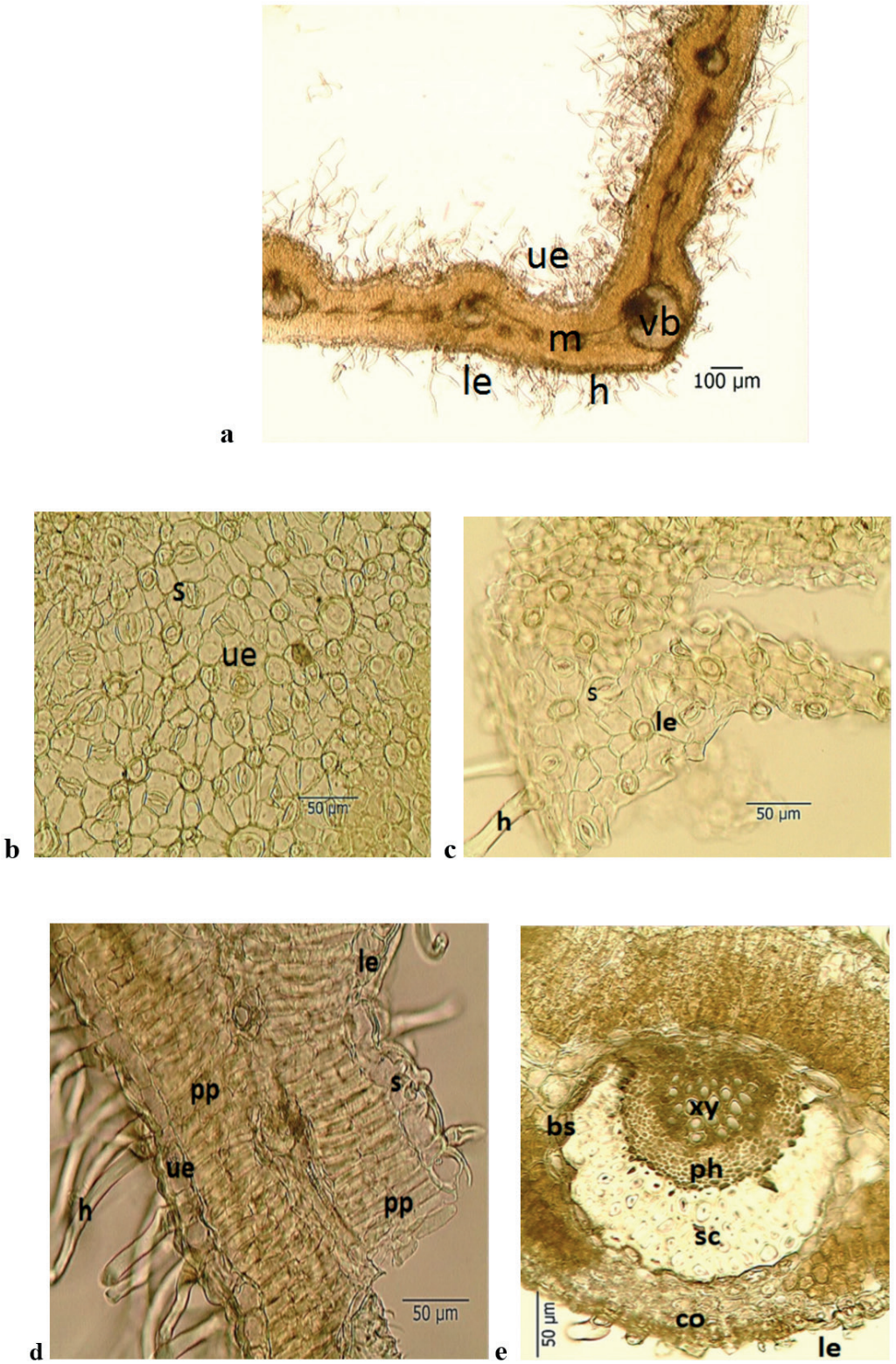

Figure 8. Transverse section of leaflet. a-general view b-upper surface c-lower surface d-mesophyll, e-midrib, bs-bundle sheat h-hair co-collenchyma s-stomata ue-upper epidermis le-lower epidermis pp-palsade parenchyma m-mesophyll ph-phloem sc- sclerenchyma xy-xylem.

4. DISCUSSION

A. tmoleus is a member section of *Pterophorus* and it is represented by two endemic varieties (var. *tmoleus* and var. *bounacanthus*) in the Flora of Turkey [1]. According to Flora, varieties separate from the shape of bracts. The shape of bracts is linear in var. *tmoleus* while it is ovate-lanceolate to orbicular shaped and bilobed in var. *bounacanthus*. In this study, morphological, anatomical and palynological properties of *Astragalus tmoleus* var. *bounacanthus* have been investigated in detail. Morphological results have been compared to the Flora of Turkey in Table 1 and some differences were observed. For example, the lengths of the leaflet and stipule are more than Flora of Turkey. Also, the length of the bracts, wing, keel, stamen, ovary, legume and seed characteristics were described for the first time in this study. All morphological images were drawn and the deficiencies in the Flora were completed.

A study is present about *A. tmoleus* var. *tmoleus* [9]. When the morphological part of this study is examined, it is seen that it is a literal translation of the plant definition in the Flora of Turkey. In conclusion, I have not formed a positive opinion about the reliability of Pirdal et al.'s study [9].

Table 1. Morphological characters of Astragalus tmoleus var. bounacanthus based on the present study and Flora of Turkey

	Astragalus tmoleus* var. *bounacanthus	**Flora of Turkey**
Leaf rachis	1.9-5 cm	2-5 cm
Leaflets	(3-) 4-6 (-7) çift	3-6 (-7) çift
	5-13 x 2.5-5 mm	4-8 mm
Stipul	9-14 x 4-7 mm	10 mm
Flower number	20-40	20-40
Bract	8-12 x 5-8 mm	-
Bracteol	7-12 x 1.5-3 (-4) mm	8-12 mm
Calyx	10-15 mm	10-15 mm
Corolla	Rose-pink	Rose-pink
Standart	12-18,5 mm	15-18 mm
Wings	12-18 mm	-
Keels	12-17 mm	-
Stamen	11-18 mm	-
Ovary	4-6 x 1,8-2,5 mm	-
Legumen	5-7 x 2-5 mm	-
Seed	(2-)2,5-3,8 x 1,5-2,5 mm	-

A. tmoleus in Flora of Turkey is defined as a species close to *A. trojanus.* However, the differences of inflorescence and the shape of bracts in species are reported. Furthermore, the leaflets of *A. tmoleus* are pilose-tomentolleus while the leaflets *A. trojanus* are pilose or glabrous. The seeds of some *Astragalus* species such as *A. tmoleus* var. *bounacanthus* are generally reniforme shaped and seed surface is rugulate or undulate-ridges [4,10-13].

The pollen grains in the Fabaceae family are simple or united. Generally, they are tricolpate, sometimes 2, 4 or 6 aperture and variable shape from peroblate to prolate. In Turkey, pollen grains of *Astragalus* species are generally stenolapynous and radial symmetry, isopolar, tricolpate and they show microreticulate ornamentation [3,11,13-18]. Our pollen findings are similar to the above evidences.

Astragalus species are xeromorphic plants that grow on stone slopes. The presence of a thick cuticula in the leaflet, dense trichomes and the lack of stomata or located at epidermis level stomata and fewness of sponge parenchymatic cells in leaflets, cushing-forming shrubs are characteristic for *A. tmoleus* var. *bounacanthus*. These features are the peculiar properties of the xeromorph plants [19]. As a result of the anatomic studies, *A. tmoleus* var. *bounacanthus* shows the characteristics of the xeromorph plants. Anomocytic types of stomata are characteristics for the Fabaceae family and this type is observed in this study [20].

Some anatomical (stem, rachis and leaflets) studies have been reported on various *Astragalus* species [9-10,21-23]. Pirdal et al. [9] are reported anatomical properties of root, stem, rachis and leaflets in endemic *A. tmoleus* var. *tmoleus*. In another study, Uysal [10] investigated stem, rachis and leaflets anatomy properties of endemic *A. trojanus.* The primary cortex structure, sclerenchyma tissue on the phloem and the presence of amylum in the piths of *A. tmoleus* var. *tmoleus* and *A trojanus* are consistent with our results.

The rachis anatomy features in an earlier studies [9-10,21-23] are similar to our findings as the shape of rachis, collenchyma tissue under the epidermis, small-big vascular bundles, vascular bundles surrounded by scleranchymatic cells, pith in a narrow area.

Leaflet anatomical properties of Pirdal et al. [9] and Uysal [10] are also supported by our leaflet anatomical results as mentioned in equifacial leaflets, anamocytic stomata, the structure of vascular bundles and the lackness of sponge parenchyma. Metcalfe and Chalk [20] recorded equifacial type in *Astragalus* species. *A. tmoleus* var. *bounacanthus*'s leaves have the same mesophyll structure.

Pirani et al. [21] had been studied the petiole anatomy of 35 *Astragalus* species in *Rhacophorus* section while Mehrabian et al. [23] had been investigated the petiole anatomy of 24 *Astragalus* species in the *Incani* section. Researchers in both studies reported two petiole types. The first type of petioles has a narrow pith area that consists of thick-walled parenchyma cells and vascular bundles are surrounded by broadly a sclerenchyma cell group. The second type has a large pith area which consists of thin-walled parenchyma cells and vascular bundles are surrounded by narrowly a sclerenchyma cell group. Our samples are similar to the first type.

5. CONCLUSION

In the present study, morphological, anatomical and pollen characteristics of endemic *A. tmoleus* var. *bounacanthus* have been investigated for the first time in this study. In morphological studies, in detail description of the plant was given were supported by drawings. Morphological characters such as the shape of paripinnate leaves, stipules and bracts, the flower number in the inflorescence, the stenonychioid type of standard and the reniform type of seed can be helpful to distinguish *A. tmoleus* var. *bounacanthus.* While the stem, leaf and rachis characteristics of the plant were examined in anatomical studies, the pollen structure of the plant was determined in palynological studies. The data obtained at this stage enrich the information about the these features of the members of the Fabaceae family and can be used in comparative studies, both between the species of the genus *Astragalus* and also with molecularly related genera.

Ethical approval

Not applicable, because this article does not contain any studies with human or animal subjects.

Author contribution

Concept: AK; Design: AK; Supervision: AK; Materials: AK; Data Collection and/or Processing: AK; Analysis and/or Interpretation: AK; Literature Search: AK; Writing: AK; Critical Reviews: AK.

Source of funding

This research received no grant from any funding agency/sector.

Conflict of interest

The author declared that there is no conflict of interest.

REFERENCES

1. Davis PH. Astragalus L. In: Davis PH, editor. Flora of Turkey and the East Aegean Islands, Vol. 3. Edinburgh: Edinburgh University Press; 1970. p. 49-253.
2. Davis PH, Mill RR, Tan K. Flora of Turkey and the East Aegean Islands, Vol. 10. Edinburgh: Edinburgh University Press; 1988. p. 114-124.
3. Atasagun B, Aksoy A, Martin E. Morphological, anatomical, palynological, karyological and ecological remarks of Astragalus argaeus (Fabaceae) endemic to Turkey. Phytotaxa. 2018;379(1):118-130. https://doi.org/10.11646/phytotaxa.379.1.10
4. Vural C, Ekici M, Akan H, Aytaç Z. Seed morphology and its systematic implications for genus Astragalus L. sections Onobrychoidei DC., Uliginosi Gray and Ornithopodium Bunge (Fabaceae). Plant Syst Evol. 2008;274:255-263. https://doi.org/10.1007/s00606-008-0025-z
5. Baytop T. Türkiye'de Bitkiler ile Tedavi. İstanbul: Nobel Tıp Kitapevleri; 1999. p. 273.
6. Tanker N, Koyuncu M, Coşkun M. Farmasötik Botanik. Ankara Üniversitesi Eczacılık Fakültesi Yayınları, No: 88. Ankara: Ankara Üniversitesi Basımevi; 2004. p. 236-237.

7. Gülcemal D, Aslanipour B, Bedir E. Secondary Metabolites from Turkish Astragalus Species. In: Ozturk M, Hakeem KR, editors. Plant and Human Health, Volume 2: Phytochemistry and Molecular Aspects. Switzerland AG: Springer Nature; 2019. p. 27. https://doi.org/10.1007/978-3-030-03344-6

8. Sargın SA. Ethnobotanical survey of medicinal plants in Bozyazı district of Mersin, Turkey. J Ethnopharmacol. 2015;173:105-126. https://doi.org/10.1016/j.jep.2015.07.009

9. Pirdal M, Özdemir F, Öztürk M. Astragalus tmoleus var. tmoleus Boiss.'in morfolojisi, anatomisi ve ekolojisi üzerine araştırmalar. Anadolu Ünv Fen Ed Fak Der. 1991;3(1):27-35.

10. Uysal İ. Astragalus trojanus endemik türünün morfolojisi, anatomisi ve ekolojisi üzerinde gözlemler. Erc Ünv Fen Bil Der. 1997;13(1):54-66.

11. Ekici M, Yüzbaşıoğlu D, Aytaç Z. Morphology, Pollen, Seed Structure and Karyological Study on Astragalus ovalis Boiss. & Balansa (Sect. Ammodendron) in Turkey. Intern J Bot. 2005;1(1):74-78. https://doi.org/10.3923/ijb.2005.74.78

12. Dural H, Tugay O, Ertuğrul K, Uysal T, Demirelma H. Astragalus turkmenensis (Fabaceae), a new species from Turkey. Ann Bot Fennici. 2007;44:399-402.

13. Dinç M, Aytaç Z, Doğu S. A new species of Astragalus (Fabaceae) from Turkey. Turk J Bot. 2013;37:841-846. https://doi.org/10.3906/bot-1212-3

14. Akan H, Tatlıdil S, Bıçakcı A. Pollen morphology of Astragalus L. Section Alopecuroidei DC. (Fabaceae) in Turkey. Intern J Bot. 2005;1(1):50-55. https://doi.org/10.3923/ijb.2005.50.58

15. Pınar NM, Ekici M, Aytaç Z, Akan H, Çeter T, Alan Ş. Pollen morphology of Astragalus L. sect. Onobrychoidei DC. (Fabaceae) in Turkey. Turk J Bot. 2009;33:291-303. https://doi.org/10.3906/bot-0808-8

16. Perveen A, Qaiser M. Pollen Flora of Pakistan-VIII Leguminosae (Subfamily: Papilianaitea). Turk J Bot. 1998;22:73-91.

17. Ekici M, Aytaç Z. Astragalus dumanii (Fabaceae) a new species from Anatolia, Turkey. Ann Bot Fennici. 2001;38:171-174.

18. Ekici M, Aytaç Z, Akan H, Pınar M. A new species of Astragalus L. (section Onobrychoidei DC.: Fabaceae) from Turkey. Bot J Linn Soc. 2008;157:741-747. https://doi.org/10.1111/j.1095-8339.2008.00828.x

19. Yentür S. Bitki Anatomisi, No: 191. İstanbul: İstanbul Üniversitesi Fen Fakültesi Yayınları; 1984. p. 405.

20. Metcalfe CR, Chalk L. Anatomy of the Dicotyledons: Volume I: Systematic Anatomy of Leaf and Stem, with a Brief History of the Subject. Oxford: Clarendon Press; 1972. p. 502-533.

21. Pirani A, Zarre S, Tillich HJ, Podlech D, Niknam V. Spine anatomy and its systematic application in Astragalus sect. Rhacophorus s. L. (Fabaceae) in Iran. Flora. 2006;201:240-247. https://doi.org/10.1016/j.flora.2005.07.006

22. Kandemir N, Korkmaz H, Engin A. The Morphological and Anatomical Properties of Astragalus barba-jovis DC. var. barba-jovis (Fabaceae). Turk J Bot. 1996;20(3):291-299. https://doi.org/10.55730/1300-008X.2641

23. Mehrabian AR, Zarre SH, Azizian D, Podlech D. Petiole anatomy in Astragalus Sect. Incani DC. (Fabaceae) in Iran (A phylogenetical approach). Iran J Bot. 2007;13(2):138-145.

ANADOLU UNIVERSITY
INSTITUTE OF HEALTH SCIENCES

European Journal of Life Sciences 2022; 1: 46-54

Research Article

Capsaicin inhibits proliferation and induces apoptosis in human lung adenocarcinoma A549 cell line

Merve Tiltay[1], Aydan Hüseynli[2], Gülşen Akalın Çiftçi[2], İ. Özkan Alataş[1]

[1]Department of Medicinal Biochemistry, Faculty of Medicine, Eskişehir Osmangazi University, Eskişehir, Turkey.
[2]Department of Biochemistry, Faculty of Pharmacy, Anadolu University, Eskişehir, Turkey.

✉ Merve Tiltay
mervetiltay@gmail.com

https://doi.org/10.55971/EJLS.1151479

Received: 30.07.2022
Accepted: 21.10.2022
Available online: 11.11.2022

ABSTRACT

Capsaicin is the main component of many hot peppers, exerts anticancer effects on various cancer cells by inducing apoptotic pathways. In addition, the ineffectiveness of this apoptotic effect of capsaicin on healthy cells provides a wide-ranging use of capsaicin. In recent years, many studies have been carried out to determine the safety of capsaicin use in lung cancer, which is a common cancer type worldwide with high mortality rates. In the present study anticancer effects of capsaicin were studied on A549 human lung adenocarcinoma cell line. Also, citotoxicity of this compound was studied on L929 mouse embryonic fibroblast cell line. Various concentration of capsaicin (3.90625-500 µM) effectively decreased cell viability in A549 cell line in a dose-dependent manner. Also, this antiproliferative effect of capsaicin was selective compared to L929 cell line. On the other hand, apoptosis inducing effects of capsaicin were studied by Annexin V-FITC and Caspase 3 assays by using IC_{50} and $IC_{50/2}$ concentrations on A549 cell by flow cytometric methods. Our results revealed that the anticancer effects induced by capsaicin on A549 cell line involved apoptosis by inducing Caspase 3 pathway.

Keywords: Capsaicin, A549, Apoptosis, Flow cytometry

1. INTRODUCTION

Lung cancer is the most common type of cancer in the globe. The impact of environmental variables is especially essential in the etiology of lung cancer, with cigarette smoke being the single most important causative agent. Other relevant concerns include radiation exposure and a variety of occupational-related hazards, the most well-known of which being asbestos. Lung cancer is classified into several histological categories, the most common of which are adenocarcinoma and squamous cell carcinoma (25-40 percent each), followed by small cell lung cancer (20-25 percent), and large cell carcinoma (20-25 percent). A succession of genetic mutations are necessary for the formation of a malignant lung carcinoma, as is the case for the majority of human cancers. K-ras mutations are thought to be particularly responsible for adenocarcinomas. Small cell lung cancer is linked to the oncogene myc, and several lung malignancies have been linked to mutations in the tumor suppressor gene p53 [1]. Various medications for molecular targeted treatment and immunotherapy have been developed and authorized for clinical use up to this point. Despite the advancement of these treatments, lung cancer remains the greatest cause of cancer-related mortality, accounting for an anticipated 1.8 million deaths in 2020. New treatment approaches are urgently required because the majority of these fatalities ultimately result from medication resistance and poor sensitivity. Recently, it has become clear that controlling the metabolism of cancer offers

great potential for combating treatment resistance and boosting medication effectiveness. The primary barriers to successful treatment include a lack of early diagnosis, a poor prognosis, the development of resistance to chemotherapeutic medicines, and a five-year survival rate of fewer than 15% of the cancer population. [2,3].

8-methyl-N-vanilyl-trans-6-nonenamide, which we know as capsaicin and is a homovalinic acid derivative is the active ingredient of Capsicum annum chili peppers. Although it is known as a spice around the world, it is used as a medicine with its anti-inflammatory, anti-analgesic, analgesic and anti-obesity effects, and it has a wide place in the literature. Cluster headaches, rheumatoid arthritis, post-mastectomy pain syndrome, diabetic neuropathy, and herpes zoster are just a few of the conditions that capsaicin has been used to treat [4]. Particularly lung cancer, have been the subject of in-depth research on the action of capsaicin, which may have anticancer and antiproliferative properties [3-5]. Most often, capsaicin-mediated cytotoxicity is linked to cancer cell apoptosis through the activation of a number of processes, such as the production of reactive oxygen species (ROS), the beginning of endoplasmic reticulum (ER) stress, and changes in protein kinases [6,7].

Both apoptosis and autophagy are tightly controlled processes involved in several crucial cellular activities, however apoptosis often serves as a mechanism for self-destruction as opposed to autophagy's cytoprotective function. Binding to death receptors starts the extrinsic pathway of apoptosis, which then activates initiator caspase-8 and effector caspases [6]. In the intrinsic pathway, the BCL-2 family proteins (Bax and Bak) assemble into oligomers in the mitochondria's outer membrane, causing cytochrome c to leak out into the intermembrane space. When cytochrome c is released, apoptosomes are formed, containing Apaf-1 and caspase-9. Caspase-9 then activates downstream caspases, such caspase-3, by proteolytic cleavage [8].

In the light of the reported data we have planned to study anticancer activity of capsaicin on A549 cell line. Capsaicin was screened to determine it's cytotoxic effects on A549 and L929 cell lines. Also apoptotic properties of it was studied on A549 human lung adenocarcinoma cell lines.

2. MATERIALS AND METHODS

2.1. Materials

The A549 cells were purchased from American Type Culture Collection (ATCC, USA). Cisplatin and capsaicin were from Sigma-Aldrich (USA), Dulbecco's Modified Eagle Medium (DMEM) was from Gibco (Brasil), fetal bovine serum (FBS) and penicillin streptomycin were from Gibco (South America, USA), Dulbecco's phosphate-buffered saline concentrate (10X) was from Biological Industries (Israel), MTT was from Alfa Aesar (Germany), and dimethylsulfoxide (DMSO) was from Sigma-Aldrich. The Annexin-V FITC/ propidium iodide (PI) apoptosis detection kit, caspase-3 kit were purchased from BD Biosciences (USA). The Annexin-V FITC were purchased from Santa Cruz Biotechnology (USA).

2.2. Methods

2.2.1. Cell Line Model

A549, human lung adenocarcima cells were maintained in Dulbecco's Modified Eagle's Medium (DMEM) and was supplemented with 10% fetal bovine serum (FBS) and antibiotics (100 µg/ ml streptomycin and 100 U/ml penicillin G) in a incubator at 37°C (5% CO_2 and 95% air).

2.2.2. MTT Assay for Cytotoxicity

This colorimetric analysis is based on the reduction of yellow tetrazolium salt (3-(4,5-dimethylthiazol-2-yl)-2,5-diphenyltetrazolium bromide or MTT) to pink formazan crystals by metabolically active cells. MTT is one of the most widely used methods work to determine for cell viability, cytotoxicity, and proliferation [9]. The A549 cells were cultured at a density of $5x10^3$ cells per well in flat bottomed 96-well plates with various concentrations (500, 125, 62.50, 31.25, 15.625, 7.813, 3.906 µM) of capsaicin and cisplatin for 24h at 37°C in a humidified atmosphere containing 5% CO_2 in air.

Various concentrations (500, 125, 62.50, 31.25, 15.625, 7.813, 3.906 µM) of capsaicin were applied to L929 cells inoculated with $5x10^3$ cells in each well in a 96-well plate, and the same incubation conditions as A549 cells were provided. At the end of incubation, MTT powder (5 mg/mL) dissolved in phosphate-buffered saline (PBS) for each well (20 µL). The cells were again incubated for 2-4 h at 37◦C. At the end of the waiting period, the media in the wells was removed and 100 µl of DMSO was added to each well. The cells were read at 540 nm using a microplate reader (Bio-Tek). Every concentration was repeated in three wells and cell viability was calculated as a percent ratio relative to control cells. According to the calculation results, the IC_{50} concentration, which provides the inhibition of 50% of the cell population, and the $IC_{50/2}$, which provides half of the 50% inhibition, were determined.

2.2.3. Flow cytometric analysis

Early evaluation of tumor response in intensively applied chemotherapy is important in terms of quality of life. Induction of apoptosis is the primary mechanism in the death of tumor cells. Annexin-V and caspase-3 assays, which have high affinity for apoptotic cells, have been frequently used imaging methods in the detection of apoptosis [10].

2.2.3.1. Annexin-V for early/late apoptosis

A549 cells were seeded in a 6-well plate at 10^5 cells/mL per well. It was incubated for 24 hours at 37°C in a humidified atmosphere containing 5% CO_2 in air. Then, determined with MTT IC_{50} and $IC_{50/2}$ doses of cisplatin and capsaicin were applied to the cells and incubated again for 24 hours. At the end of this period, the cells on the plate were removed and placed in flow tubes, centrifuged at 1200 rpm for 4 minutes. After centrifugation, the supernatant was carefully discarded, washed with 1 ml of cold 1X PBS, centrifuged again, and this was done twice. After centrifugation, the supernatant was removed and 100 µl of the assay buffer prepared as 1X was poured into each flow tube and pipetted slowly. Then 5 µl Annexin-V and 5 µl of PI dyes were added and incubated in the dark for 15 min. At the end of this period, 400 µl of assay buffer was added and analyzed. After centrifugation, the supernatant was discarded and 100 µl of the assay buffer prepared as 1X was poured into each flow tube and pipetted slowly. Then, 5 µl of Annexin-V and 5 µl of PI dyes were added and left in the dark for 15 minutes. At the end of this period, 400 µl of assay buffer was added and analyzed by flow cytometry (CytoFLEX Beckman Coulter) using FACS Diva Version 6.1.1. Software.

2.2.3.2. Analyses for Caspase-3

A549 cells were seeded in a 6-well plate at 10^5 cells/mL per well. It was incubated for 24 hours at 37°C in a humidified atmosphere containing 5% CO_2 in air. Cells were treated with calculated IC_{50} and $IC_{50/2}$ doses of cisplatin and capsaicin for 24 hours. Then, the cells on the plate were removed and placed in flow tubes and centrifuged at 1200 rpm for 4 minutes. After centrifugation, the supernatant was carefully removed and washed with 1 ml of cold 1X PBS, centrifuged again, this procedure was done twice. After centrifugation, the supernatant was discarded and 500 µl of Cytofix/Cytoperm solution was added to each tube and the tubes were kept on ice for 20 min. At the end of this period, it was centrifuged again. The supernatant was discarded, 500 µl of Permwash solution was added to each tube and centrifuged again, this process was repeated twice. The solution prepared by adding 20 µl of antibody into 100 µl of 1X Perm/Wash solution was added to the tubes and the cells were incubated for 30 minutes at room temperature. At the end of this period, it was centrifuged, the supernatant was discarded and 1 ml of Permwash solution was added and centrifuged again. Finally, 0.5 ml of Permwash was added and analyzed by flow cytometry (CytoFLEX Beckman Coulter) using FACS Diva Version 6.1.1. Software.

3. RESULTS AND DISCUSSION

3.1. MTT assay for cytotoxicity

In our study, the cytotoxic and apoptotic effects of capsaicin on A549 lung adenocarcinoma cells were investigated using in vitro MTT, Annexin V-FITC, and Caspase-3 assays. Cytotoxicity and IC_{50} values for cisplatin and capsaicin in A459 and L929 cells were determined by MTT analysis. (Tables 1 and 2). The dose and percent viability values used in the analysis are as shown in the Figures 1 and 2.

Table 1. IC_{50} and $IC_{50/2}$ dose chart for capsaicin and cisplatin for A549 cells

	IC_{50} (µM)	$IC_{50/2}$ (µM)
Cisplatin	59,233 ±	29,617 ±
Capsaicin	183,268 ±	91,634 ±

Table 2. IC_{50} table of capsaicin for L929 and A549 cells

	L929 cells	A549 cells
IC_{50} (µM)	245.569 ±	183.268 ±

These cell lines were treated with a wide range of concentrations of capsaicin and cisplatin (500, 250, 125, 62.50, 31.25, 15.625, 7.8125, 3.9063 µM) for 24 h (Table 1). Capcaicin inhibited A549 cell viabilities in a dose and time dependent manner (Figure 1). IC_{50} values of capsaicin and cisplatin were determined in A549 cells as 183,268 µM and 59,233 µM for 24h respectively (Table 1). Also, IC_{50} value of capcaicin was determined in L929 cells as 245.569 µM for 24h (Table 2). The viability of cells was decreased when the dose of capsaicin was increased (Figures 1 and 2). In the previous studies with different cell lines have obtained results supporting our findings. Liu and his colleagues (2022) discovered that IC_{50} value of capsaicin was 200 µM in A549 cells for 48 h. whereas the need was 100 µM for NCI-H23 cells for obtaining IC_{50} value [9]. The value was established to be approximately 200µM for 24 h for A549 cell lines by Lewinska and her co-workers similar as in our study [10]. Through the MTT assay, we found IC_{50} value of capsaicin as 183,268 µM in A549 cells for 24 h. On the other hand different cancer cell lines exhibit differential sensitivity to capsaicin, suggesting that the capcaisin effects vary based on the cell type. For example, the IC_{50} of capsaicin in human leukemia H60 cell was found to be 100µM for 24 hours [11], while the IC_{50} value of capsaicin was found to be 200µM for 24 hours in human glioblastoma cells [12], while the IC_{50} value of capsaicin in breast cancer cell was found to be 200µM for 72 hours [13]. On the other hand, we used L929 cells to examine selectivity of capsaicin. The IC_{50} value of capsaicin was 245.569 µM for 24 h. in L929 cell line (Table 2 and Figure 2). This result shows that capsaicin had selective antiproliferative activity against A549 cell line.

3.2. Flow cytometric analyses by annexinV-FITC

After the A549 cells were incubated with capsaicin and cisplatin at IC_{50} and $IC_{50/2}$ doses for 24 hours, reading was performed on the flow cytometry device (Beckman Coulter) using Cytoflex Software by applying the kit procedure (BD, Pharmingen). After this MTT result we examined mechanism of action of cell death on A549 cells caused by capsaicin. IC_{50} and $IC_{50/2}$ values of capsaicin were used to determine

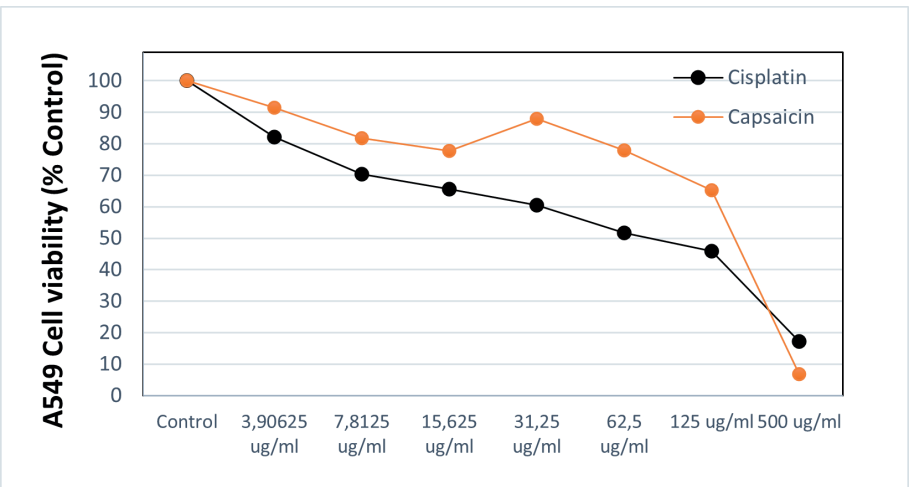

Figure 1. Dose-dependent percent viability graph of capsaicin and cisplatin on A549 cells. Cytotoxic effects of cisplatin and capsaicin on A549 cells are adenocarcinomic human alveolar basal epithelial cells after 24 hours incubation. The dose-percentage viability graph according to the effects of capsaicin and cispilatin was determined by calculating with MTT analysis.

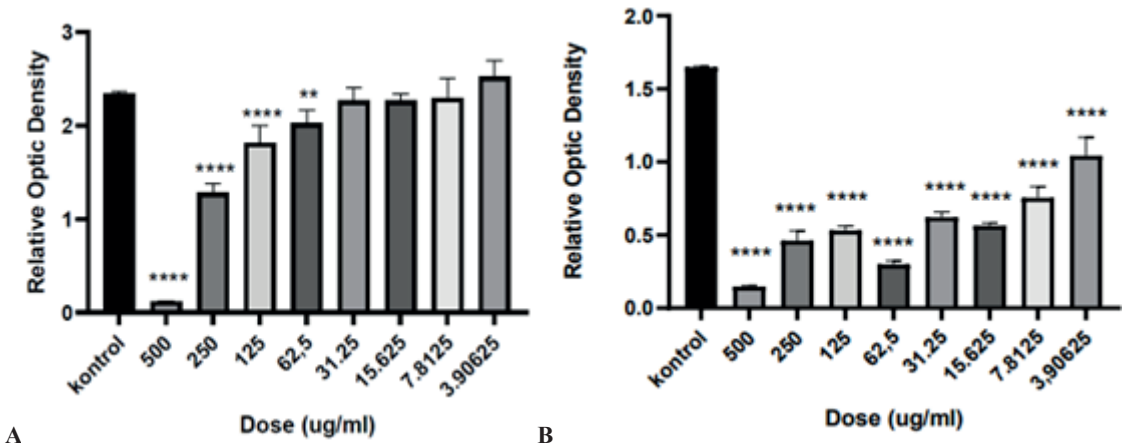

Figure 2. (A) After MTT analysis % viability ratio of capsaicin on A549 cell line after 48 hours of incubation, B) % viability rate of cisplatin on A549 cell line after 48 hours of incubation. (data recorded as mean ± SD). **p < 0.0045, ****p<0.0001 significantly different from control.

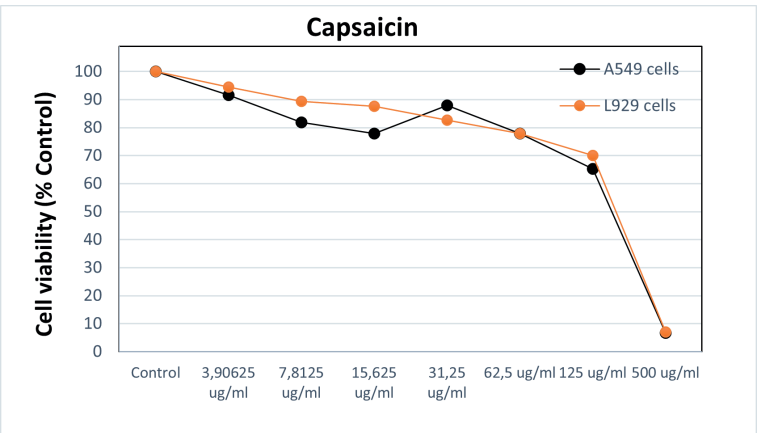

Figure 3. Dose-dependent percent viability graph of capsaicin on L929 and A549 cells. Capsaicin was also used on L929 murine fibroblast cells and compared with A459 cells to establish a control group while determining the reliable IC50 dose. data were obtained as a result of MTT analysis.

apoptotic effects of capsaicin (Figure 3, Table 3). Annexin-V binding capacity was examined by flow cytometry by applying capsaicin on the A549 cell line. After incubation of A549 cells with different concentrations of capsaicin (91.634 ve 183.268 µM), early apoptotic cell percentages were determined as 6.87 and 9.74 (Figure 3, Table 3). In addition, the percentages of late apoptotic cells were detected as %1.27 and %2.58 in incubations with different concentrations of capsaicin (Figure 3, Table 3). These results indicate that increasing capkaicin concentrations on A549 cells induce apoptosis, which includes morphological and biochemical changes. Thus, Capsaicin is identified as an effective

Table 3. Percents of typical quadrant analysis of annexin V-FITC/propidium iodide flow cytometry of A549 cells treated with the capsaicin and cisplatin

Groups	% Early	% Late	% Viable
Control (untreated)	4.39	1.22	94.39
Capsaicin $IC_{50/2}$ dose treated cells	6.87	1.27	91.84
Capsaicin IC_{50} dose treated cells	9.74	2.58	84.0
Cisplatin $IC_{50/2}$ dose treated cells	28.52	25.31	46.15
Cispaltin IC_{50} dose treated cells	50.30	35.24	14.43

apoptosis-inducing agent in different cell lines. But, its mechanism of action varies depending on cell line types. Also, doses of capsaicin used for increasing apoptosis percentages varies in different studies. In human nasopharyngeal carcinoma cells, apoptosis percentages were measured as 60% at 150µM concentration of capsaicin for 24 h [14]. In another study carried out by Leea et al. (2000) the apoptotic cell range of human glioblastoma cells were 57.2% at 200 µM of capsaicin for 24 h [12]. Also, Chou et all. (2009) showed that 200 µM of capsaicin caused 59.2% apoptotic cell percentage rate in MCF-7 cells for 24 hours [15].

3.3. Flow cytometric analyses of caspase-3 activation

The cells that were seeded in 6-plate plates were incubated for 24 hours by applying the active ingredients at the IC_{50} and $IC_{50/2}$ doses we determined. After the incubation period, readings were made with flow cytometer Beckman Coulter using Cytoflex Software by applying the kit procedure (BD, Pharmingen). Successful administration with chemotherapeutic agents is largely dependent on their ability to trigger cell death in tumor cells, and the inducing of apoptosis is mostly involved in the caspase dependent pathway [16]. It was observed that capsaicin had a dose-dependent effect on the A549 cell line, reducing caspase-3 activity (Table 4, Figure 4). Caspases regulates different biochemical pathways and morphological structures such as cell cycle regulation signaling pathways DNA condensation, fragmentation and membrane blebbing [17,18] and Caspase-3 activation was observed by capsaicin on different cell types in A549 cells [19], colon carcinoma cells [20], human renal carcinoma [21].

3.4. Statistical analysis

Percent inhibition and IC50 dosing were calculated based on the control group. All calculated data were expressed as the mean±standart error of mean (SEM) from 3 times repetition within the experiments. Data were calculated on Microsoft Excel software using a sigmoidal dose-response hill curve.

Table 4. Percent of quadrant analysis of active Caspase-3 staining by flow cytometry of A549 cells treated with the compounds

Groups	Caspase 3 positive % (+) cells	Caspase 3 negative % (-) cells
Control (untreated)	98.55	1.45
Capsaicin $IC_{50/2}$ dose treated cells	98.31	1.69
Capsaicin IC_{50} dose treated cells	95.98	4.01
Cisplatin $IC_{50/2}$ dose treated cells	77.22	22.75
Cisplatin IC_{50} dose treated cells	72.18	27.75

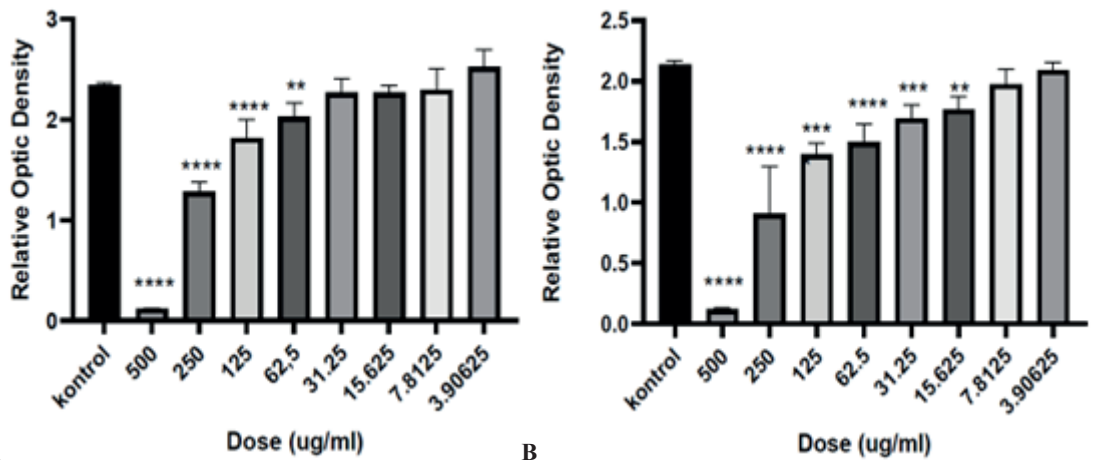

Figure 4. A) After MTT analysis % viability ratio of capsaicin on A549 cell line after 48 hours of incubation, B) % viability rate of capsaicin on L929 cell line after 48 hours of incubation. (data recorded as mean ± SD). **p < 0.0045, ***p<0.0005, ****p<0.0001 significantly different from control.

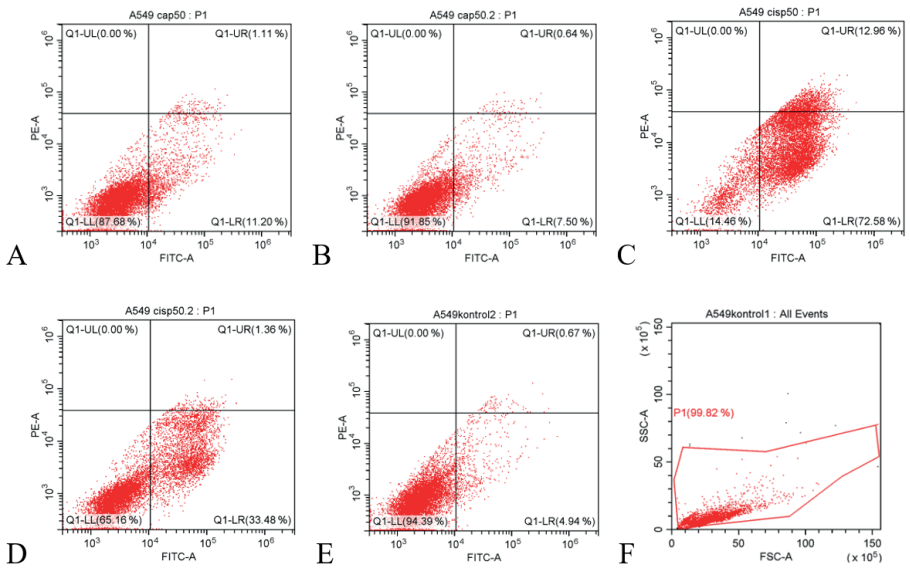

Figure 5. Flow cytometric analysis of A549 cells treated with IC50 and IC50/2 concentrations of the capsaicin and cisplatin. A549 cells were cultured for 24 hours in medium with 183.263 and 91.634 µM of capsaicin and 59.233 and 29.617 µM for cisplatin. At least 10.000 cells were analyzed per sample, and quadrant analysis was performed. Q1-LR: Early apoptotic cell percantages, Q1-UR: late apoptotic cell percentages, Q1-UL: Necrotic cell percentages, Q1-LL: viable cell percentages. A) Master gate selected from the cell population, B) Control group, C) Apoptotic effect of capsaicin IC50 dose, D) Apoptotic effect of capsaicin IC50/2 dose, E) Apoptotic effect of cisplatin IC50 dose, F) Apoptotic effect of cisplatin IC50/2 dose.

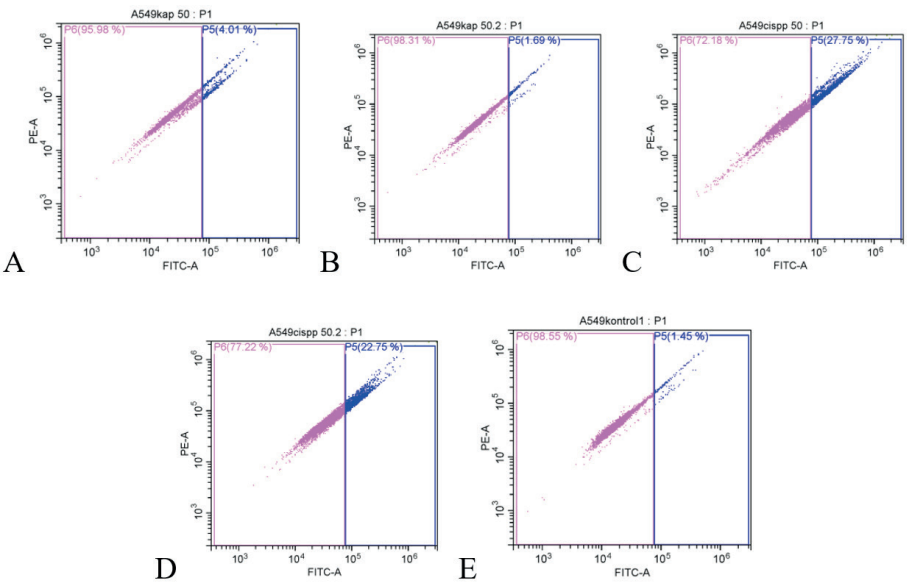

Figure 6. Flow cytometric analysis of caspase-3 activity of A549 cancer cells treated with IC50 and IC50/2 concentrations of the capsaicin and cisplatin. A549 cells were cultured for 24 hours in medium with 183.263 and 91.634 µM values of capsaicin and 59.233 and 29.617 µM for cisplatin. At least 10.000 cells were analyzed per sample, and quadrant analysis was performed. The portion (%) of cell number is shown in each quadrant. P5 shows Caspase 3 negative (-) cell percentages. P6 shows Caspase 3 positive (+) cell percentages. Controls: untreated control cells. A) Caspase-3 activity at IC50 dose of capsaicin, B) Caspase-3 activity at IC50/2 dose of capsaicin, C) Caspase-3 activity at IC50 dose of cisplatin, D) Caspase-3 activity at IC50 dose of cisplatin, E) Control Group.

4. CONCLUSION

According to our results, capsaicin has a high antiproliferative effect on the A549 cell line. These effects were found to be dose dependent. Also, capsaicin caused apoptotic cell death in A549 cells. It was determined that this effect was shown in the caspase-3 pathway, which plays an active role on the apoptotic mechanism. With this study, it is thought that capsaicin may be effective on the tumor. Although we have determined that capsaicin is effective on apoptosis in the light of the data we have obtained, more studies are needed to reveal and interact with other mechanisms.

Ethical approval

Not applicable. Because in this article only cell lines were used that were obtained from ATCC.

Author contribution

Concept: MT, AH, GAÇ, İÖA; Design: MT, AH, GAÇ; Materials: MT, AH, GAÇ; Data Collection and/or Processing: MT, AH, GAÇ; Analysis and/or Interpretation: MT, AH, GAÇ; Literature Search: MT, AH, GAÇ; Writing: MT, AH, GAÇ, İÖA; Critical Reviews: MT, AH, GAÇ, İÖA.

Source of funding

This research received no grant from any funding agency/sector.

Conflict of interest

The authors declared that there is no conflict of interest.

REFERENCES

1. Wolff H, Saukkonen K, Anttila S, Karjalainen A, Vainio H, Ristimäki A. Expression of cyclooxygenase-2 in human lung carcinoma. Cancer Res. 1998;58(22):4997-5001. https://www.researchgate.net/publication/237264292
2. Parashar P, Tripathi CB, Arya M, et al. A synergistic approach for management of lung carcinoma through folic acid functionalized co-therapy of capsaicin and gefitinib nanoparticles: Enhanced apoptosis and metalloproteinase-9 down-regulation. Phytomedicine. 2019;53:107-123. https://doi.org/10.1016/j.phymed.2018.09.013
3. Han TH, Park MK, Nakamura H, Ban HS. Capsaicin inhibits HIF-1α accumulation through suppression of mitochondrial respiration in lung cancer cells. Biomed Pharmacother. 2022;146:112500. https://doi.org/10.1016/j.biopha.2021.112500
4. Merritt JC, Richbart SD, Moles EG, et al. Anti-cancer activity of sustained release capsaicin formulations. Pharmacol Ther. 2022;238:108177. https://doi.org/10.1016/j.pharmthera.2022.108177
5. Lewinska A, Jarosz P, Czech J, et al. Capsaicin-induced genotoxic stress does not promote apoptosis in A549 human lung and DU145 prostate cancer cells. Mutat Res Genet Toxicol Environ Mutagen. 2015;779:23-34. https://doi.org/10.1016/j.mrgentox.2015.02.003
6. Lee YH, Chen HY, Su LJ, Chueh PJ. Sirtuin 1 (SIRT1) Deacetylase Activity and NAD^+/NADH Ratio Are Imperative for Capsaicin-Mediated Programmed Cell Death. J Agric Food Chem. 2015;63(33):7361-7370. https://doi.org/10.1021/acs.jafc.5b02876
7. Pramanik KC, Srivastava SK. Apoptosis signal-regulating kinase 1-thioredoxin complex dissociation by capsaicin causes pancreatic tumor growth suppression by inducing apoptosis. Antioxid Redox Signal. 2012;17(10):1417-1432. https://doi.org/10.1089/ars.2011.4369
8. Cooper GM, Hausman RE. The cell: A molecular approach. Sunderland (MA): Sinauer Associates; 2013. p. 686-687.
9. Liu XY, Wei DG, Li RS. Capsaicin induces ferroptosis of NSCLC by regulating SLC7A11/GPX4 signaling in vitro. Sci Rep. 2022;12(1):11996. https://doi.org/10.1038/s41598-022-16372-3
10. Lewinska A, Chochrek P, Smolag K, Rawska E, Wnuk M. Oxidant-based anticancer activity of a novel synthetic analogue of capsaicin, capsaicin epoxide. Redox Rep. 2015;20(3):116-125. https://doi.org/10.1179/1351000214Y.0000000113
11. Tsou MF, Lu HF, Chen SC, et al. Involvement of Bax, Bcl-2, Ca2+ and caspase-3 in capsaicin-induced apoptosis of human leukemia HL-60 cells. Anticancer Res. 2006;26(3A):1965-1971.
12. Lee YS, Nam DH, Kim JA. Induction of apoptosis by capsaicin in A172 human glioblastoma cells. Cancer Lett. 2000;161(1):121-130. https://doi.org/10.1016/S0304-3835(00)00608-X

13. Chang HC, Chen ST, Chien SY, Kuo SJ, Tsai HT, Chen DR. Capsaicin may induce breast cancer cell death through apoptosis-inducing factor involving mitochondrial dysfunction. Hum Exp Toxicol. 2011;30(10):1657-1665. https://doi.org/10.1177/0960327110396530

14. Lin YT, Wang HC, Hsu YC, Cho CL, Yang MY, Chien CY. Capsaicin Induces Autophagy and Apoptosis in Human Nasopharyngeal Carcinoma Cells by Downregulating the PI3K/AKT/mTOR Pathway. Int J Mol Sci. 2017;18(7):1343. https://doi.org/10.3390/ijms18071343

15. Chou CC, Wu YC, Wang YF, Chou MJ, Kuo SJ, Chen DR. Capsaicin-induced apoptosis in human breast cancer MCF-7 cells through caspase-independent pathway. Oncol Rep. 2009;21(3):665-671. https://doi.org/10.3892/or_00000269

16. Hickman JA, Potten CS, Merritt AJ, Fisher TC. Apoptosis and cancer chemotherapy. Philos Trans R Soc Lond B Biol Sci. 1994;345(1313):319-325. http://doi.org/10.1098/rstb.1994.0112

17. Mancini M, Nicholson DW, Roy S, et al. The caspase-3 precursor has a cytosolic and mitochondrial distribution: implications for apoptotic signaling. J Cell Biol. 1998;140(6):1485-1495. https://doi.org/10.1083/jcb.140.6.1485

18. Çiftçi GA, Işcan A, Kutlu M. Escin reduces cell proliferation and induces apoptosis on glioma and lung adenocarcinoma cell lines. Cytotechnology. 2015;67(5):893-904. https://doi.org/10.1007/s10616-015-9877-6

19. Hansakul P, Aree K, Tanuchit S, Itharat A. Growth arrest and apoptosis via caspase activation of dioscoreanone in human non-small-cell lung cancer A549 cells. BMC Complement Altern Med. 2014;14:413. https://doi.org/10.1186/1472-6882-14-413

20. Kim MY, Trudel LJ, Wogan GN. Apoptosis induced by capsaicin and resveratrol in colon carcinoma cells requires nitric oxide production and caspase activation. Anticancer Res. 2009;29(10):3733-3740.

21. Liu T, Wang G, Tao H, et al. Capsaicin mediates caspases activation and induces apoptosis through P38 and JNK MAPK pathways in human renal carcinoma. BMC Cancer. 2016;16(1):790. https://doi.org/10.1186/s12885-016-2831-y

ANADOLU UNIVERSITY
INSTITUTE OF HEALTH SCIENCES

European Journal of Life Sciences 2022; 1: 55-62

Research Article

Geographical impact on essential oil composition of endemic *Salvia absconditiflora* collected from different parts of Turkey

Ayla Kaya[1], Süleyman Doğu[2], Betül Demirci[3]

[1]Anadolu University, Faculty of Pharmacy, Department of Pharmaceutical Botany, Eskişehir, Turkey.
[2]Necmettin Erbakan University, Meram Vocational School, Department of Medical and Aromatic Plants, Konya, Turkey.
[3]Anadolu University, Faculty of Pharmacy, Department of Pharmacognosy, Eskişehir, Turkey.

✉ Ayla Kaya
aykaya@anadolu.edu.tr

https://doi.org/10.55971/EJLS.1140861

Received: 05.07.2022
Accepted: 19.10.2022
Available online: 14.11.2022

ABSTRACT

This study was carried out to determine the content of the essential oils of *Salvia absconditiflora* Greuter & Burdet populations which are naturally found in Mediterranean, Iran-Turan and Euro-Sibirya phytogeographical regions. *S. absconditiflora* plant samples were collected from eight different provinces (Aksaray, Kahramanmaraş, Karaman, Kayseri, Konya, Niğde, Nevşehir and Yozgat) of Turkey. Essential oils of plant samples were isolated by the hydro-distillation method using a Clevenger-type apparatus and the components were determined by GC-FID and GC-MS analysis. Although the major components of *S. absconditiflora* were found as α-pinene, camphene, 1,8-cineole, camphor, and borneol in almost all samples β-pinene, β-caryophyllene, bornyl acetate, caryophyllene oxide, β-eudesmol and valeranone were recorded as the other important components in some samples.

Keywords: Essential oil, Hydro-distillation, GC-FID, GC-MS, *Salvia absconditiflora*

1. INTRODUCTION

The genus *Salvia* L. (sage) is a member of Lamiaceae family, is a widespread group consisting of 900 species in the world and 96 species and 4 subspecies in Flora of Turkey, 51 % of which are endemic. *Salvia* members produce many secondary metabolites including terpenes and phenolics [1,2]. Many species of the genus are used the pharmaceutical and cosmetics industry and drink as herbal tea in many countries. They have important medicinal uses including treatment for colds, aches, microbial infections, malaria, cancer, Alzheimer's, and cardiovascular disease all over the World. They are generally known under the name "adaçayi" and are widely used as herbal tea. Also, they are used against wounds, inflammation and skin diseases in folk medicine [1,3,4].

Salvia absconditiflora Greuter & Burdet (Synonym: *S. cryptantha* Montbret & Aucher ex Bentham) is an aromatic, endemic and perennial herbaceous plant. *S. absconditiflora*, known locally name "karaşalba" in Turkey, is characterized by branched to dendroid hairs and sessile glands [5]. The tea prepared with the aerial parts of *S. absconditiflora* is used for stomach disorders and the plant is also utilized as a colorant [1]. It is reported that *S. absconditiflora* has antitumoral potential against breast cancer [6].

There are some reports in the literature about the chemical composition of *S. absconditiflora* essential oil [4,7-12]. Here, we present our findings on the chemical constituents of the essential oils obtained from *S. absconditiflora* grown in eight different provinces of Anatolia.

2. MATERIALS AND METHODS

2.1. Plant Material

The samples were collected from the following regions of Turkey by Süleyman Doğu. The voucher specimens (S.D.) are deposited at the Herbarium of the Department of Biology, Necmettin Erbakan University, Konya, Turkey. Detailed information was given in Table 1.

2.2. Isolation of essential oil

The samples were isolated by hydro-distillation for 3 hours, using a Clevenger-type apparatus. The obtained oil was dried over anhydrous sodium sulfate and stored at +4°C in the dark until analyzed and tested. The essential oils were analyzed by GC-FID and GC-MS systems, simultaneously. All processes were performed with reference to Kaya et al. [13].

2.3. Identification of the Components

Wiley GC/MS Library, MassFinder 4 Library and in-house "Başer Library of Essential Oil Constituents" built up by genuine compounds and components of known oils were used for the identification [14,15].

3. RESULTS AND DISCUSSION

The essential oils were obtained by hydro-distillation from air-dried aerial parts of *S. absconditiflora* collected from eight different regions in Turkey. The essential oils were subsequently analyzed by GC-FID and GC-MS and the individual identified components and their relative percentages are given in Table 2.

Sixty-eight compounds were identified from the oil of Niğde representing 97.0% of the total oil, forty compounds were identified from the oil of Aksaray representing 97.9% of the total oil, sixty-four compounds were identified from the oil of Kahramamaraş representing 96.5% of the total oil, forty-nine compounds were identified from the oil of Yozgat representing 95.3% of the total oil, sixty-nine compounds were described from the oil of Nevşehir representing 94.4% of the total oil, fifty-three compounds were identified from the oil of Konya representing 99.8% of the total oil, ninety-four compounds were identified from the oil of Karaman representing 96.2% of the total oil, and seventy-five compounds were identified from the oil of Kayseri representing 97.9% of the total oil.

α-Pinene (7.9-26.7%) and camphene (5.1-14.3%) were found as major components in all samples. Other main compounds were 1,8-cineole (6.1-36.4%) (except Kahramanmaraş, Yozgat, and Nevşehir samples) camphor (5.0-19.4%), (except Aksaray and Yozgat samples) and borneol (5.5-20.9%) (except Aksaray, Yozgat, and Nevşehir samples). However, β-pinene (5.5% and 15.9%) for Nevşehir and Aksaray samples, bornyl acetate (5.6%) for Yozgat sample, β-caryophyllene (6.1%) for Kahramanmaraş sample, caryophyllene oxide (8.2%) for Nevşehir sample, valeranone (6.0-7.8%) for Nevşehir and Yozgat samples, and β-eudesmol (5.4%) for Kahramanmaraş sample were found as the other important components.

In an earlier study, Bayrak and Akgül (1987) reported that twenty-two constituents of the oil of *S. crypthantha* contained borneol (24.8%), camphor (17.5%), 1,8-cineole (10.4%) and α-pinene (5.8%) as main components [7].

Table 1. Information on *S. absconditiflora* samples

Cities	Collection place	Altitude	Coll. date	Coll. number
Niğde	Ulukışla	1400 m	22.05.2018	S.D. 3025
Aksaray	Nevşehir 23. km	1053 m	20.05.2018	S.D. 3020
Kahramanmaraş	Göksun 27. km	850 m	22.05.2018	S.D. 3024
Yozgat	Çayıralan-Çandır 3. km	1450 m	20.05.2018	S.D. 3023
Nevşehir	Avanos	1100 m	20.05.2018	S.D. 3021
Konya	Konya-Beyşehir 10. km	1100 m	17.05.2018	S.D. 3018
Karaman	Ermenek Balkusan vadisi	1300 m	18.05.2018	S.D. 3019
Kayseri	Özvatan-Çayıralan 8.km	1300 m	20.05.2018	S.D. 3022

Table 2. The composition of the essential oils of *S. absconditiflora*

RRI	Compound	1	2	3	4	5	6	7	8	IM
1014	Tricyclene	0.2	0.3	0.7	0.5	0.7	0.4	0.5	0.5	MS
1032	*α*-Pinene	**15.3**	**24.8**	**14.5**	**16.9**	**26.7**	**11.5**	**20.3**	**7.9**	RRI, MS
1035	*α*-Thujene	0.1	0.5	0.1	0.3	0.4	0.1	0.2	0.1	RRI, MS
1072	*α*-Fenchene	0.2	-	0.1	0.1	-	-	0.1	0.1	RRI, MS
1076	Camphene	**6.2**	**5.1**	**12.6**	**12.7**	**14.3**	**8.5**	**9.3**	**10.5**	RRI, MS
1093	Hexanal	-	-	-	-	-	-	tr	-	RRI, MS
1118	*β*-Pinene	1.1	**15.9**	2.6	3.4	**5.5**	3.2	3.1	1.6	RRI, MS
1132	Sabinene	0.1	-	0.1	0.2	0.6	0.1	0.1	0.1	RRI, MS
1135	Thuja-2,4(10)-diene	-	-	tr	-	-	-	tr	-	MS
1174	Myrcene	0.2	2.2	0.6	0.6	1.1	1.7	1.5	0.5	MS
1176	*α*-Phellandrene	0.1	-	0.1	0.1	0.1	0.1	0.1	0.1	RRI, MS
1188	*α*-Terpinene	0.1	0.3	0.2	0.3	0.2	0.3	0.2	0.2	RRI, MS
1194	Heptanal	-	-	-	-	-	-	tr	-	RRI, MS
1203	Limonene	0.9	3.8	1.3	2.5	2.3	1.2	3.6	0.8	RRI, MS
1213	1,8-Cineole	**12.9**	**6.1**	4.7	2.3	2.0	**36.4**	**6.8**	**13.2**	RRI, MS
1244	2-Pentyl furan	tr	0.2	tr	0.1	0.1	-	0.1	-	MS
1246	*(Z)-β*-Ocimene	0.1	-	0.4	0.3	1.0	0.3	0.3	0.1	MS
1255	*γ*-Terpinene	0.2	0.4	0.3	0.5	0.3	0.4	0.3	0.3	RRI, MS
1266	*(E)-β*-Ocimene	tr	-	0.1	tr	0.2	tr	tr	tr	MS
1280	*p*-Cymene	0.5	1.9	0.6	0.9	0.1	0.6	0.5	0.5	RRI, MS
1290	Terpinolene	0.1	0.1	0.1	0.2	0.2	0.1	0.2	0.1	RRI, MS
1304	1-Octen-3-one	-	-	-	-	-	-	tr	-	MS
1353	Hexyl isobutyrate	-	-	0.1	-	0.2	-	0.1	0.1	MS
1360	1-Hexanol	-	-	-	-	-	-	-	0.3	MS
1386	1-Octenyl acetate	-	-	-	-	-	-	tr	-	MS
1393	3-Octanol	-	-	-	-	-	-	tr	-	MS
1400	Nonanal	-	-	0.1	-	0.1	-	tr	-	MS
1424	Hexyl butyrate	-	-	0.1	-	0.2	-	-	-	MS
1438	Hexyl 2-methyl butyrate	-	-	0.1	-	0.3	-	0.1	0.2	MSMS
1452	*α,p*-Dimethylstyrene	tr	-	-	-	-	-	tr	-	MS
1452	1-Octen-3-ol	0.1	-	tr	0.1	-	0.1	0.3	0.1	MS
1466	*α*-Cubebene	-	-	0.1	-	0.1	0.1	0.1	-	MS
1474	*trans*-Sabinene hydrate	-	-	0.1	-	-	0.1	0.1	0.1	MS
1483	Octyl acetate	-	-	tr	-	0.1	-	tr	-	RRI, MS
1493	*α*-Ylangene	-	-	0.1	-	-	0.1	0.1	-	MS
1496	2-Ethyl hexanol	-	-	-	-	-	-	-	0.2	MS
1497	*α*-Copaene	0.1	4.4	1.9	1.1	0.5	0.3	1.1	0.8	RRI, MS
1519	Hexyl valerate	-	-	-	-	-	-	-	0.1	MS
1528	*α*-Bourbonone	-	-	-	-	-	-	0.1	-	MS
1532	Camphor	**11.5**	1.6	**9.0**	4.6	**5.0**	**16.5**	**15.8**	**19.4**	RRI, MS
1544	*α*-Gurjunene	0.1	-	-	-	-	-	0.1	-	MS
1547	Octyl isobutyrate	-	-	-	-	-	-	-	0.1	MS
1553	Linalool	0.5	-	0.2	-	-	0.2	0.1	0.1	RRI, MS
1556	*cis*-Sabinene hydrate	-	-	-	-	-	0.1	0.1	0.1	MS

Table 2. Continued

RRI	Compound	1	2	3	4	5	6	7	8	IM
1559	*β*-Maaliene	0.1	-	-	-	-	-	-	-	MS
1562	Isopinocamphone	tr	-	-	-	-	-	0.1	-	RRI, MS
1562	Octanol	0.1	-	0.1	-	0.2	0.1	0.1	0.9	RRI, MS
1571	*trans-p*-Mentha-2-en-1-ol	-	-	-	-	-	-	0.2	-	MS
1586	Pinocarvone	0.1	-	-	-	-	-	-	-	RRI, MS
1588	Bornyl formate	-	-	-	-	-	-	0.1	-	MS
1589	Aristolene	0.1	-	-	-	-	-	-	-	MS
1589	*β*-Ylangene	-	-	0.1	-	-	-	-	-	MS
1590	Bornyl acetate	2.2	1.1	1.7	**5.6**	0.8	1.7	2.5	1.1	RRI, MS
1597	*β*-Copaene	-	-	0.2	-	0.1	0.1	0.2	-	MS
1600	*β*-Elemene	-	-	-	-	tr	-	-	-	RRI, MS
1610	Calarene	0.1	-	-	-	-	-	0.3	-	MS
1611	Terpinen-4-ol	1.0	-	0.3	-	0.1	0.7	0.3	0.7	RRI, MS
1612	*β*-Caryophyllene	3.3	4.3	**6.1**	4.9	3.1	0.3	0.8	4.7	RRI, MS
1620	Selina-5,11-diene	0.3	-	-	-	-	0.1	-	-	MS
1623	Octyl butyrate	-	-	0.1	-	0.2	-	-	-	MS
1628	Aromadendrene	2.8	1.0	-	0.2	-	0.4	-	0.8	MS
1634	Octyl 2-methyl butyrate	-	-	-	-	0.1	-	-	0.1	MS
1638	*cis-p*-Mentha-2-en-1-ol	-	-	-	-	-	-	0.1	-	MS
1648	Myrtenal	-	-	-	-	-	-	0.1	0.1	MS
1650	*γ*-Elemene	-	-	-	-	0.1	-	-	-	MS
1651	Bornyl isobutyrate	0.1	-	-	-	-	-	0.2	-	MS
1659	*γ*-Gurjunene	0.1	-	-	-	-	-	0.2	-	MS
1661	Alloaromadendrene	0.2	-	-	-	-	-	0.1	0.1	MS
1670	*trans*-Pinocarveol	0.2	-	-	-	-	-	0.3	0.1	RRI, MS
1682	*δ*-Terpineol	-	-	0.1	-	-	0.1	-	-	MS
1683	*trans*-Verbenol	0.1	-	-	-	-	-	-	-	RRI, MS
1687	*α*-Humulene	0.2	1.0	0.3	0.3	0.2	0.2	tr	0.5	RRI, MS
1688	Selina-4,11-diene	-	-	tr	-	-	-	-	0.1	MS
1698	Myrtenyl acetate	0.1	-	-	-	-	-	-	-	MS
1704	*γ*-Muurolene	-	0.8	1.0	1.0	0.3	0.4	0.9	-	MS
1706	*α*-Terpineol	-	-	0.2	-	-	0.1	-	0.4	RRI, MS
1708	Ledene	1.0	-	-	-	-	0.2	0.3	tr	MS
1709	*α*-Terpinyl acetate	-	-	-	-	0.3	-	-	-	RRI, MS
1718	4,6-Guaiadiene	-	-	-	-	-	-	-	0.1	MS
1719	Borneol	**20.9**	0.6	**5.5**	3.5	1.0	**6.1**	**9.8**	**9.1**	RRI, MS
1726	Germacrene D	-	0.6	-	-	1.5	-	-	-	MS
1740	*α*-Muurolene	-	tr	-	0.2	0.1	0.1	-	-	MS
1742	*β*-Selinene	0.6	-	1.7	1.0	0.2	0.2	0.9	0.9	MS
1744	*α*-Selinene	0.5	-	0.8	0.5	0.1	0.1	0.6	0.4	MS
1751	Carvone	-	-	-	-	-	-	-	-	RRI, MS
1755	Bicyclogermacrene	0.2	1.1	-	-	-	-	0.6	-	MS
1755	*β*-Curcumene	-	-	-	-	-	-	-	0.2	MS
1758	*cis*-Piperitol	-	-	-	-	-	-	0.1	-	RRI, MS

Table 2. Continued

RRI	Compound	1	2	3	4	5	6	7	8	IM
1770	Isobornyl isovalerate	0.1	-	-	-	-	-	0.3	-	MS
1773	*δ*-Cadinene	0.1	1.5	1.2	1.6	0.5	0.5	1.3	0.4	MS
1776	*γ*-Cadinene	-	1.4	0.4	0.5	0.1	0.1	0.4	0.2	MS
1786	*ar*-Curcumene	-	-	-	-	-	-	-	0.7	MS
1796	Selina-3,7(11)-diene	-	-	0.8	-	-	0.5	1.0	1.4	MS
1799	Cadina-1,4-diene	-	-	0.1	-	-	-	0.1	-	MS
1804	Myrtenol	1.8	-	-	-	-	0.2	0.9	0.6	MS
1805	*α*-Campholene alcohol	0.1	-	0.3	-	-	0.2	0.5	0.7	MS
1849	Calamenene	-	1.5	0.4	0.3	0.4	0.1	0.3	0.2	MS
1868	*(E)*-Geranyl acetone	-	-	0.1	-	0.1	-	-	-	MS
1900	*epi*-Cubebol	-	-	0.1	-	-	-	0.1	-	MS
1941	*α*-Calacorene	-	-	0.2	-	-	0.1	0.1	-	MS
1957	Cubebol	-	0.6	0.2	-	0.2	-	tr	0.1	MS
1958	*(E)-β*-Ionone	0.1	-	-	-	-	-	-	-	MS
2001	Isocaryophyllene oxide	-	-	-	-	0.1	-	-	-	MS
2008	Caryophyllene oxide	1.0	2.9	2.4	1.8	**8.2**	0.1	0.3	0.8	RRI, MS
2012	Maaliol	0.2	-	-	-	-	-	-	-	MS
2033	*epi*-Globulol	0.2	-	-	-	-	-	-	-	MS
2037	Salvial-4(14)-en-1-one	-	-	-	-	0.3	-	-	-	MS
2045	Humulen epoxide-I	tr	-	-	-	-	-	-	-	MS
2050	*(E)*-Nerolidol	-	0.8	-	-	-	-	0.1	-	MS
2057	Ledol	-	-	-	-	-	-	tr	0.1	MS
2071	Humulen epoxide-II	-	1.3	0.2	-	0.2	0.1	-	0.2	MS
2073	*β*-Caryophyllene alchool	-	-	0.1	-	0.1	-	-	0.1	MS
2088	1-*epi*-Cubenol	-	tr	0.1	0.2	-	-	0.1	-	MS
2096	*cis*-Sesquisabinene hydrate	-	-	-	-	-	-	-	0.3	MS
2098	Globulol	0.8	-	-	-	-	-	-	-	MS
2104	Viridifrolol	0.2	-	-	0.9	0.8	2.7	-	2.5	MS
2130	Salviadienol	-	-	-	-	0.6	-	0.1	-	MS
2131	Hexahydrofarnesyl acetone	-	tr	-	0.3	0.3	-	0.2	-	MS
2144	Rosifoliol	0.3	-	-	-	-	-	tr	0.1	MS
2144	Spathulanol	0.8	2.3	-	-	-	-	1.2	-	MS
2145	Valeranone	1.1	2.5	3.6	**7.8**	**6.0**	1.3	-	2.8	MS
2161	Muurola-4,10(14)dien-1-ol	-	-	0.3	-	-	-	0.1	-	MS
2170	*β*-Bisabolol	-	-	-	-	-	-	-	1.8	RRI, MS
2178	*T*-Cadinol	-	1.1	0.2	-	-	-	-	-	MS
2185	*γ*-Eudesmol	-	-	-	-	-	-	0.4	-	MS
2186	Eugenol	-	-	-	-	-	-	0.1	-	RRI, MS
2187	*T*-Cadinol	-	-	-	-	-	-	-	0.1	MS
2204	Eremoligenol	-	-	-	-	-	-	0.2	-	MS
2209	T-Muurolol	-	-	0.1	-	0.1	-	0.1	-	MS
2210	Copaborneol	-	-	-	-	-	-	-	0.2	MS
2210	Hinesol	-	-	-	-	-	-	0.2	-	MS
2211	Clovenol	0.3	-	0.3	-	-	-	-	0.1	MS

Table 2. Continued

RRI	Compound	1	2	3	4	5	6	7	8	IM
2250	*α*-Eudesmol	0.7	tr	1.7	1.0	0.5	0.2	1.5	0.8	RRI, MS
2256	Cadalene	-	-	-	-	-	-	0.1	0.1	MS
2257	*β*-Eudesmol	2.0	1.7	**5.4**	3.8	-	0.4	1.8	2.6	RRI, MS
2269	Guaia-6,10(14)dien-4*β*-ol	-	-	-	0.7	0.1	-	-	-	MS
2273	Porosadienol	-	-	0.6	-	0.1	-	0.3	0.7	MS
2278	Torilenol	-	-	-	-	0.6	-	-	-	MS
2296	*(Z)-α-trans*-Bergamotol acetate	-	1.4	-	-	-	-	-	-	RRI, MS
2316	Caryophylladienol I	0.5	-	0.1	0.5	0.3	-	-	-	MS
2324	Caryophylladienol II	-	-	1.0	-	0.3	-	-	0.4	MS
2369	Eudesma-4(15)7-dien-1-*β*-ol	-	-	-	-	1.2	-	-	-	MS
2389	Caryophyllenol I	1.3	-	1.9	1.4	0.2	-	0.1	0.8	MS
2392	Caryophyllenol II	0.5	-	1.1	0.9	0.7	-	-	0.5	MS
2500	Pentacosane	-	-	-	0.2	-	-	-	-	RRI, MS
2512	Benzophenone	-	-	-	-	-	-	-	0.1	RRI, MS
2622	Phytol	-	-	-	1.0	0.2	-	0.1	-	MS
2679	Manool	-	-	4.0	4.0	1.0	-	-	-	RRI, MS
2700	Heptacosane	-	-	-	1.1	-	-	-	-	RRI, MS
2931	Hexadecanoic acid	tr	0.8	0.5	2.4	0.5	-	0.1	-	RRI, MS
	Total	**97.0**	**97.9**	**96.5**	**95.3**	**94.4**	**99.8**	**96.2**	**97.9**	

RRI: Relative retention indices calculated against *n*-alkanes; %: calculated from FID data; tr: Trace (< 0.1 %); IM: Identification method based on the relative retention indices (RRI) of authentic compounds on the HP Innowax column; MS, identified on the basis of computer matching of the mass spectra with those of the Wiley and MassFinder libraries and comparison with literature data; 1-Niğde, 2-Aksaray, 3-Kahramanmaraş, 4-Yozgat, 5-Nevşehir, 6-Konya, 7-Karaman, 8-Kayseri.

Başer et al. (1995) reported that there were sixty constituents in *S. crypthantha* oil gathered from Ankara and Eskişehir. The main components were 1,8-cineole (15.7-37.1%), camphor (5.95.0-13.04%), α-pinene (1.0-11.9%) and camphene (0.9-7.7%) [8].

Akgül et al. (1999) published that the essential oil of *S. crypthantha* collected from Karaman was characterized by camphor (18.1%), 1,8-cineole (17.8%), bornyl acetate (11.4%) and borneol (5.8%) as main components [9]. These results are similar to our Karaman samples except bornyl acetate.

Tepe et al. (2004) published the essential constituents of the oil of *S. crypthantha* samples collected from Sivas. Fifty-three constituents were identified representing 90.9% of the total oil and α-pinene (18.1 %), eucalyptol (15.3%), camphor (7.7%), camphene (6.4%) and borneol (4.8%) were found as main compounds in *S. crypthantha* oil [10].

Saadia et al. (2010) reported that sixteen constituents were described representing 98.5% of the oil of *S. crypthantha* at the flowering stage collected from Derbent, Konya. This oil is characterised by the monoterpene hydrocarbons and oxygenated monoterpenes, and camphor (25.6 %), 1,8-cineole (20.3 %), β-pinene (12.8 %), *n*-hexane (10.6 %), heptane (8.9 %), borneol (5.1 %) and α-pinene (4.1 %) were detected as main constituents [11]. β-pinene, n-hexane and heptane were not recorded as main constituents in our Konya samples.

İpek et al. (2012) studied essential oils of *Salvia cryptantha* and they reported nine components of the Ereyli, Konya sample were detected representing 94.75% of the oil. Valencene (31.80%), eucalyptol (23.61%), and β-pinene (15.63%) were found to be the major compounds [12]. When we compare our findings with this study, only eucalyptol as the main compound shows similarity with our Konya results.

Doğan et al. (2017) published that the essential oil of *S. crypthantha* was collected from Darende, Sivas. Sixty-three constituents were described representing 98.7% of the oil and 1.8-cineole (21%), camphor (19.1%), α-pinene (12.5%), and camphene (8.7%) were found as the main compounds [4].

Comparing our results on *S. absconditiflora* essential oil with those previously reported, we can see that they are almost notably the same. However, there are still some differences. These variations may be due to geographical, edaphic and climatological factors, the time of flowering, drying conditions, and made of distillation. These factors also play a role in the composition of the oil. Moreover, due to the frequent occurrence of chemotypes in Lamiaceae species, it is possible to see different compositions in oils of the same plant species [11,13].

4. CONCLUSION

Hydro-distilled eight *S. absconditiflora* oils were analyzed by using GC-FID and GC-MS systems, simultaneously. A total of 68, 40, 64, 49, 69, 53, 94 and 75 components were identified from the essential oils of *S. absconditiflora* respectively, which represented 97, 97.9, 96.5, 95.3, 94.4, 99.8, 96.2 and 97.9% of the oils. Borneol, α-pinene, camphene, camphor, and 1,8-cineole were described as the main compounds for the oil of almost all samples. However β-pinene, β-caryophyllene, bornyl acetate, caryophyllene oxide, β-eudesmol and valeranone are the other important components in some other samples.

Ethical approval

Not applicable, because this article does not contain any studies with human or animal subjects.

Author contribution

Concept: AK; Design: AK; Supervision: AK, BD; Materials: SD; Data Collection and/or Processing: AK, BD; Analysis and/or Interpretation: AK, BD; Literature Search: AK; Writing: AK; Critical Reviews: AK, BD.

Source of funding

This research received no grant from any funding agency/sector.

Conflict of interest

The authors declared that there is no conflict of interest.

REFERENCES

1. Uysal S. A comparative study of three drying methods on the phenolic profile and biological activities of Salvia absconditiflora. J Food Measurement and Characte. 2019;13:162-168. https://doi.org/10.1007/s11694-018-9929-7
2. Yilar M, Bayar Y, Abaci Bayar AA. Allelopathic and Antifungal potentials of endemic Salvia absconditiflora Greuter & Burdet collected from different locations in Turkey. Allelopathy Journal. 2020;49(2):243-256. https://doi.org/10.26651/allelo.j/2020-49-2-1268
3. Tenore GC, Ciampaglia R, Arnold NA, et al. Antimicrobial and antioxidant properties of the essential oil of Salvia lanigera from Cyprus. Food Chem Toxicol. 2011;49(1):238-243. https://doi.org/10.1016/j.fct.2010.10.022
4. Doğan G, Hayta Ş, Demirpolat A, Bağcı E. Composition of the Essential Oil of Endemic Salvia cryptantha (Lamiaceae) Montbret & Aucher Ex Bentham from Turkey. Hacettepe J Biol & Chem. 2017;45(3):315-320. https://doi.org/10.15671/HJBC.2017.171
5. Davis PH. Flora of Turkey and the East Aegean Islands (Vol. 7). Edinburgh: Edinburgh University Press; 1982. p. 400-461.
6. Özer H, Altun A, Saraydın SU, et al. Antitumoral effects of Salvia absconditiflora Greuter & Burdet syn. Salvia cryptantha Montbret & Aucher ex Benth. on breast cancer. Indian J Traditional Knowle. 2013;12(3):390-397.
7. Bayrak A, Akgül A. Composition of essential oils of Turkish Salvia species, Phytochemistry. 1987;26:846-847. https://doi.org/10.1016/S0031-9422(00)84802-5
8. Başer KHC, Beis SH, Özek T. Composition of the Essential Oil of Salvia cryptantha Montbret et Aucher ex Benth. from Turkey. Journal of Essential Oil Research. 1995;7:113-114. https://doi.org/10.1080/10412905.1995.9698479
9. Akgül A, Özcan M, Chialva F, Monguzzi F. Essential Oils of Four Turkish Wild-Growing Labiatae Herbs: Salvia cryptantha Montbr. et Auch., Satureja cuneifolia Ten., Thymbra spicata L. and Thymus cilicicus Boiss. et Bal. Journal of Essential Oil Research. 1999;11:209-214. https://doi.org/10.1080/10412905.1999.9701113

10. Tepe B, Donmez E, Unlu M, et al. Antimicrobial and antioxidative activities of the essential oils and methanol extracts of Salvia cryptantha (Montbret et Aucher ex Benth.) and Salvia multicaulis (Vahl). Food Chem. 2004;84:519-525. https://doi.org/10.1016/S0308-8146(03)00267-X

11. Saadia Z, Özcan MM, Bagci Y, et al. Chemical Composition of the Essential oil of Salvia cryptantha. J Essent Oil Bearing Plants. 2010;13(2):200-204. https://doi.org/10.1080/0972060X.2010.10643812

12. İpek A, Gürbüz B, Bingöl MÜ, et al. Comparison of essential oil components of wild and field grown Salvia cryptantha Montbert & Aucher ex Benthan, in Turkey. Turk J Agric For. 2012;36:668-672. https://doi.org/10.3906/tar-1201-4

13. Kaya A, Dinç M, Dogu S, Demirci B. Compositions of essential oils of Salvia adenophylla, Salvia pilifera, and Salvia viscosa in Turkey. Journal of Essential Oil Research. (2017); 29(3):233-239. http://doi.org/10.1080/10412905.2016.1216901

14. McLafferty FW, Stauffer DB. The Wiley/NBS Registry of Mass Spectral Data. New York: J. Wiley and Sons; 1989.

15. Hochmuth DH. MassFinder 4.0, Hochmuth Scientific Consulting, Hamburg, Germany; 2008.

ANADOLU UNIVERSITY
INSTITUTE OF HEALTH SCIENCES

European Journal of Life Sciences 2022; 1: 63-69

Research Article

Antimicrobial and antioxidant activities of *Sideritis lanata* L. extracts

Zeynep Gülcan[1], Nagehan Saltan[1], Gökalp İşcan[2], Mine Kürkçüoğlu[2], Yavuz Bülent Köse[1]

[1]Anadolu University, Faculty of Pharmacy, Department of Pharmaceutical Botany, Eskişehir, Turkey.
[2]Anadolu University, Faculty of Pharmacy, Department of Pharmacognosy, Eskişehir, Turkey.

✉ Zeynep Gülcan
zgulcan@anadolu.edu.tr

https://doi.org/10.55971/EJLS.1181461

Received: 28.09.2022
Accepted: 08.11.2022
Available online: 17.11.2022

ABSTRACT

Sideritis L. (Lamiaceae) is represented by 45 species in Flora of Turkey. *Sideritis lanata* L. (Hairy ironwort) is located in the north-west, west, south-west and central Anatolia. Mountain tea (*Sideritis plants*) is used as a traditional remedy against common cold and gastrointestinal disorders. Its beneficial properties are attributed to its rich bioactive constituents. In this study, the antioxidant activities of the extracts of Sideritis lanata prepared using different solvents (*n*-hexane, ethyl acetate, and 70% ethanol) from the aerial parts were determined by DPPH· scavenging effect assay. Also; determined of the antimicrobial activity of S. lanata extracts against 4 bacteria and 5 *Candida* species. Dried aerial parts of *Sideritis* were subjected to hydrodistillation and the oil obtained was analyzed by using GC and GC/MS. *S. lanata* extracts prepared with 70% ethanol was found to have a higher DPPH· scavenging activity (IC_{50}= 0.241 mg/mL) than extracts prepared with other solvents. All extracts showed generally weak inhibitory effects (500-8000 µg/mL, MIC) against bacterial strains. Inhibitory doses against the tested *Candida* species were determined between 125-4000 µg/mL. The 70% ethanol extract of *S. lanata* inhibited *Candida tropicalis* (ATCC 750) (MIC: 125 µg/mL).

Keywords: Antimicrobial Activity, Antioxidant activity, Essential oil, GC-GC/MS, *Sideritis lanata*

1. INTRODUCTION

There are 45 species (60 taxa) of *Sideritis* in Turkey, and the endemism rate is quite high with approximately 80% [1]. *Sideritis* species has been used in traditional medicine for cough, cold, gastrointestinal disorders, antiseptic, anti-inflammatory, antirheumatic, antimicrobial and insecticidal [2]. *Sideritis* genus contains chemical components such as flavonoids, terpenes, coumarins, essential oils, lignans, iridoids, and sterols. Diterpenes, flavonoids, and essential oils are found in almost every species of *Sideritis* and are the main compounds responsible for *in vivo* and *in vitro* pharmacological activities [3]. *Sideritis lanata* L. (Lamiaceae) is a species that spreads mainly in the Mediterranean region. The plant is locally known as "İpek çayı" in Turkey [4]. The chemical composition of *S. lanata* has been extensively studied in 2000. The major components of *S. lanata* were found as hexadecanoic acid (10.67%) and spathulenol (9.45%) [5]. With spectroscopic methods; 7-*O*-β-D-glucopyranosylchrysoeriol, 7-*O*-[(6‴-O-acetyl)-β-D-allopyranosyl (1→2)-β-D-glucopyranosyl] hypolaetin , 7-*O*-[(6‴-O-acetyl)-β-D-allo pyranosyl (1→2)-β-D-glucopyranosyl] hypolaetin-3′-methyl

ether and 7-*O*-[(6‴-O-acetyl)-β-D-allopyranosyl (1→2)-β-D-glucopyranosyl] isoscutellarein and a new iridoid diglucoside 10-0-(*E*)-p coumaroylmelittoside and a new flavone glucoside and a new flavone glucoside 7-O- (6″-O-Acetyl-)-β-glucopyranosylchrysoeriol have been identified by Alipieva et al. [6]. The antimicrobial activity of *S. lanata* essential oil was studied by the disc diffusion method. The essential oil has been shown to have a strong antimicrobial effect against Gram-positive bacteria, especially methicillin-resistant *Staphylococcus aureus* (MRSA) and oxacillin-resistant coagulase-negative *Staphylococcus epidermidis*. *Bacillus cereus, Bacillus subtilis*, and *Micrococcus luteus* were found sensitive bacteria to the essential oil of *S. lanata* [7]. As far as we know when the literature was reviewed, the antioxidant effect of *S. lanata* has not been reported before. Our study, *S. lanata* with $DPPH^{\cdot}$ scavenging activity method, can be considered the first report in terms of antioxidant activity. In addition, in our study, the antibacterial effect was studied by selecting different strains from other antimicrobial activity experiments.

2. MATERIALS AND METHODS

2.1. The Plant Material

S. lanata was collected from Kutlu, Bolvadin/ Afyonkarahisar in Turkey on June 2021. The voucher specimen has been deposited at the Herbarium in the Anadolu Unıversity, Eskisehir, Turkey (Voucher specimen no: ESSE 15820). The plant material was identified by Prof. Dr. Yavuz Bulent KOSE.

2.2. Isolation of Essential Oil

Essential oil of the aerial parts was extracted by hydrodistillation Clevenger apparatus method.

2.3. GC Analysis

GC analyses were performed using an Agilent 6890N GC system. FID temperature was set to 300°C and the same operational conditions were applied to a triplicate of the same column used in GC/MS analyses. Simultaneous auto-injection was employed to obtain equivalent retention times. Relative percentages of the separated compounds were calculated from integration of the peak areas in the GC-FID chromatograms.

2.4. GC/MS Analysis

The GC/MS analysis was carried out with an Agilent 5975 GC-MSD system (Agilent, USA; SEM Ltd., Istanbul, Turkey). Innowax FSC column (60m x 0.25mm, 0.25μm film thickness) was used with helium as carrier gas (0.8 mL/min.). GC oven temperature was kept at 60°C for 10 min and programmed to 220°C at a rate of 4°C/min, and kept constant at 220°C for 10 min and then programmed to 240°C at a rate of 1°C/min. Split ratio was adjusted 40:1. The injector temperature was at 250°C. The interphase temperature was at 280°C. MS were taken at 70 eV. Mass range was from *m/z* 35 to 450.

2.5. Identification of Compounds

The components of essential oils were identified by comparison of their mass spectra with those in the in-house Baser Library of Essential Oil Constituents, Adams Library [8], MassFinder Library [9], Wiley GC/MS Library [10], and confirmed by comparison of their retention indices. These identifications were accomplished by comparison of retention times with authentic samples or by comparison of their relative retention index (RRI) to a series of n-alkanes. Alkanes were used as reference points in the calculation of relative retention indices (RRI) [11]. Relative percentage amounts of the separated compounds were calculated from FID chromatograms.

2.6. Extract Preparation

Three extracts of the species with 70% ethanol, *n*-hexane, and ethyl acetate were prepared. The aerial parts of the plant were cut into small pieces. A weight of 18 grams was taken from the sample and 200 mL of solvent was added. Samples were left to maceration in a shaker (Orbital) at 150 rpm at room temperature for 48 hours. After the macerated were filtered through filter paper, their solvents were removed with a rotavapor under reduced pressure.

70% ethanolic extract was obtained by lyophilizer. The extracts, freed from their solvents, were stored in the refrigerator at +4 ºC until use.

2.7. Antioxidant activity

The antioxidant activities of the extracts of *S. lanata* prepared using different solvents (*n*-hexane, ethyl acetate and 70% ethanol) from the aerial parts were determined by DPPH· radical scavenging effect assay. The methods of Kumarasamy et al. were used for the determination of DPPH· scavenging effect [12].

2.8. Determination of Total Phenolic Content Using the Folin-Ciocalteu Reagent (FCR)

The extract's total amount of phenol was determined as equivalent to mg Gallic Acid using the Folin-Ciocalteu reagent method. The method based on the Folin-Ciocalteu reagent (FCR), known as the total phenolic reagent, determines the reducing capacity of the sample. Gallic acid is usually used as the standard compound and results are given as gallic acid equivalent (mg/mL). Different solutions of gallic acid were prepared in the concentration range of 1-0.03 mg/mL, absorbance values were recorded at 760 nm, and the calibration equation was determined by drawing the concentration absorbance graph of gallic acid. Samples absorbance measurements at 760 nm were taken and compared with the gallic acid calibration curve. TFC (Total Phenolic Content) was calculated as gallic acid equivalents (GAE) in mg/g dry weight of plant material. A reagent mixture without extract and solvent was used as a control. Three parallel experiments were performed and the results were given as mean values [13,14].

2.9. Antimicrobial activity

Determination of the antimicrobial activity of *S. lanata* extracts against 4 bacteria *(Staphylococcus aureus (*ATCC 6538), *Pseudomonas aeruginosa* (ATCC 27853), *Serratia marcescens* (NRRL B-2544), *Klebsiella pneumoniae* (NCTC 9633) and 5 *Candida* species (*Candida utilis* (NRRL Y- 900), *Candida albicans (*ATCC 90028), *Candida tropicalis* (ATCC 750), *Candida parapsilosis* (ATCC 22019), *Candida krusei* (ATCC 6258). The minimum inhibitory (MIC) concentrations of the extracts were determined using standard protocols (CLSI M7-A7 and M27-A2).

3. RESULTS AND DISCUSSION

3.1. Chemical composition of the essential oil

The yield of essential oil obtained from the aerial parts of the plant was found to be 1.05%. The essential oil was analyzed by GC and GC/MS. 27 compounds representing 89.1% of the essential oil was characterized with unknown (29.7%), Phytol (15.7%), 9-geranyl-p-cymene (7.5%) and β-caryophyllene (6.1%) as major constituents. The chemical components of *S. lanata* essential oil analyzed by GC-GC/MS are shown in Table 1. In a study on *Sideritis* in Greece, it was observed that the essential oil was quite dense (46.3%) in terms of sesquiterpenes. It has fewer components in terms of monoterpenes (3.5%) and diterpenes (10.9%). The major components were spathulenol (12.7%), β-phellandrene (3.5%), and ent-2α hydroxy-8(14),5-pimaradiene (9.7%), respectively [15]. In a study on some *Sideritis* species (*S. scardica, S. raeseri, S. syriaca, S. taurica* and *S. lanata*) in the Balkan Peninsula the most abundant hydroxycinnamic acid derivative in *Sideritis* was 5-caffeoylquinic acid. In most samples, including *S. lanata*, 5-caffeoylquinic acid was the only hydroxycinnamic acid detected [16]. The aerial parts of *S. albiflora* Hub.-Mor. essential oil were analyzed simultaneously by GC-FID and GC-MS. 88 compounds representing 88.2% of the essential oil were characterized by germacrene D (23.5%), β-caryophyllene (13.6%), caryophyllene oxide (8.0%), and hexadecanoic acid (3.8%) as major constituents [17].

3.2. Antimicrobial activity

All extracts showed generally weak inhibitory effects (500-8000 µg/mL, MIC) against bacterial strains (Table 2). Inhibitory doses against the tested *Candida* species were determined between

125-4000 µg/mL. A 70% ethanol extract of *S. lanata* inhibited *Candida tropicalis* (ATCC 750) at a dose of 125 µg/mL (MIC) (Table 3).

In a study done in 2005, the essential oil of *S. lanata* (5 µl) had no effect on Gram-negative bacteria, whereas it was observed to have an inhibitory effect on all Gram-negative organisms at 25 µL. 10 and 25 µl essential oils of *S. lanata* were observed to have a significant effect on all Gram-positive bacteria used in the study [7].

Table 1. The chemical components of *Sideritis lanata* essential oil

RRI	Compounds	Sideritis %	Grup	IM
1400	Nonanal	0.5	D	MS
1452	1-Octen-3-ol	0.5	D	t_R, MS
1495	Bicycloelemene	1.0	ST	MS
1541	Benzaldehyde	2.0	D	MS
1589	β-Ylangene	0.5	ST	MS
1612	β-Caryophyllene	6.1	ST	t_R, MS
1722	2-Undecanol	0.2	D	MS
1726	Germacrene D	1.3	ST	MS
1755	Bicyclogermacrene	3.0	ST	t_R, MS
1800	Octadecane	0.4	D	t_R, MS
1958	(*E*)-β-Ionone	1.4	D	MS
2096	Elemol	3.2	OST	MS
2131	Hexahydrofarnesyl acetone	1.5	D	MS
2144	Spathulenol	0.8	OST	t_R, MS
2227	Unknown*	29.7	DT	MS
2239	Carvacrol	tr	OMT	t_R, MS
2255	α-Cadinol	0.7	OST	t_R, MS
2300	Tricosane	0.3	D	t_R, MS
2312	9-Geranyl-p-cymene	7.5	D	MS
2384	Farnesyl acetone	0.6	D	MS
2486	8-α-Acetoxyelemol	1.4	D	MS
2500	Pentacosane	0.8	D	t_R, MS
2622	Phytol	15.7	ODT	MS
2700	Heptacosane	3.4	D	t_R, MS
2781	Geranyl geraniol	4.3	OST	MS
2931	Hexadecanoic acid	2.9	D	MS
3000	Tricontane	0.8	D	MS
	OST Oxygenated sesquiterpenes	9.94		
	OMT Oxygenated monoterpenes	tr		
	DT Diterpene	32.82		
	ODT Oxygenated diterpene	17.35		
	D-Others	26.74		
	ST Sesquiterpene hydrocarbons	13.15		
	Total %	90.5		

RRI: Relative retention indices calculated against n-alkanes; %: calculated from the FID chromatograms; tr: Trace (<0.1 %). Identification method (IM): t_R, identification based on the retention times of genuine compounds on the HP Innowax column; MS, identified on the basis of computer matching of the mass spectra with those of the in-house Baser Library of Essential Oil Constituents, Adams, MassFinder and Wiley libraries and comparison with literature data.

* *m/z*: 272 [M+] (18), 188 (47), 187 (26), 159 (25), 132 (48), 133 (22), 121 (69), 119 (100), 107 (24), 105(49), 93 (43), 91 (36), 81 (22), 79 (22), 69 (67), 41 (26).

Table 2. Anticandidal effect of *Sideritis lanata* extracts (µg/mL)

	H	EtOAc	EtOH	AMP-B	Keto
Candida utilis NRRL Y-900	250	500	500	1	0.5
Candida albicans ATCC 90028	2000	2000	4000	1	0.5
Candida tropicalis ATCC 750	250	250	125	2	0.25
Candida parapsilosis ATCC 22019	2000	2000	4000	2	0.125
Candida krusei ATCC 6258	500	1000	2000	1	1

AMP-B: Amphotericin B, Keto: Ketoconazole, H: *Sideritis lanata n*-hexane extract, EtOAc: Extract with ethyl acetate, EtOH: Extract with ethanol 70%.

Table 3. Antibacterial effect of *Sideritis lanata* extracts (µg/mL)

	n-Hexane	Ethyl acetate	Ethanol %70	Ampicillin	Chloramphenicol
Staphylococcus aureus ATCC 6538*	500	2000	>8000	1	4
Pseudomonas aeruginosa ATCC 27853	4000	4000	>8000	>64	8
Serratia mar-cescens NRRL B-2544	4000	4000	>8000	>64	4
Klebsiella pne-umoniae NCTC 9633	4000	4000	8000	>16	2

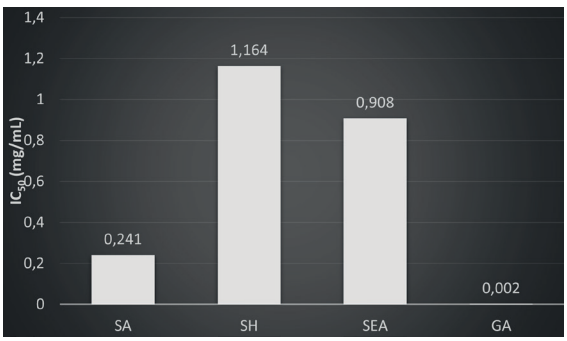

Figure 1. The ability of extract in scavenging DPPH· scavenging activity.

SA: 70% ethanol extract of *S. lanata*, SH: n-Hexane extract of *S.lanata*, SEA: Ethyl acetate extract of *S. lanata*, GA: Gallic acid.

Table 4. DPPH· scavenging activity of *S. lanata*

Extracts	DPPH· test IC_{50} (mg/mL)
Ethanol %70	0.241 ±0.115
n-Hexane	1.164 ±0.197
Ethyl acetate	0.908 ±0.165
Gallic acid	0.002 ±0.001

mg GAE/g extract: Total phenols expressed as gallic acid equivs milligrams of gallic acid per gram (dry weight) of extract

3.3. Antioxidant activity

S. lanata extracts prepared with 70% ethanol was found to have a higher DPPH· radical scavenging activity (0.241 mg/mL) than extracts prepared with other solvents (Table 4). To the best of our knowledge, there is no study on the antioxidant activity of *Sideritis lanata*. *S. syriaca, S. scardica*, and *S. montana* were extracted with different solvents in Bulgaria. Their antioxidant activities were determined by the 2,2-diphenyl 1-picrylhydrazyl (DPPH**)** radical scavenging method. The most effective extracts were found to be methanol, butanol and ethyl acetate extracts [18]. In the other study, antioxidant activity tests were carried out by lipid oxidation of liposomes using the TBA (Thiobarbituric acid test) method. TLC was used as a screening method to evaluate the antioxidant activities of freeze-dried extracts of *Sideritis* species with the DPPH· test. Antioxidant

activities of lyophilized extracts obtained from the aerial parts of 17 species (18 taxa) of which 15 taxa of *Sideritis* are endemic were compared. The highest activity in TBA method was observed in *S. brevibracteata* extract (IC_{50} mg/ml = 0.16). However, in general, the antioxidant values of the species were low. In the study, it was decided that teas made with these species did not have much antioxidant activity [19].

3.4. Folin-Ciocalteu reagent (FCR) and the total phenolic method (Total Phenol Quantification) Results

The total amount of phenol contained in the extracts obtained from the aerial parts of the plants was determined by a spectrophotometric method using the Folin-Ciocalteu reagent. The total phenol amounts of the extracts are given in Table 5 as equivalent to Gallic acid. The calibration curve and curve equation of the gallic acid used in the calculations are shown in Figure 2. According to the findings, the highest total phenol content (61.1±0.03 mg GAE/g extract) was determined in the ethanolic extract in *S. lanata* samples. Extracts with *n*-hexane were found to be weak in terms of phenolic compounds. It was determined that the total amount of phenol was also high in the ethanol extract of *S. lanata*, which has the highest antioxidant activity. These results revealed that there is a correlation between total phenol content and antioxidant activity.

Table 5. The total amount of phenol equivalent to Gallic acid contained in *S. lanata* extracts

SA	61.1±0.03mg GAE/g ekstre
SH	12.25±0.04 mg GAE/g ekstre
SEA	20.82±0.02 mg GAE/g ekstre

GAE: phenol amount equivalent to mg GAE/g extracted Gallic acid, SA: 70% ethanol extract of *S. lanata*, SH: n-hexane extract of *S.lanata*, SEA: Ethyl acetate extract of *S. lanata*.

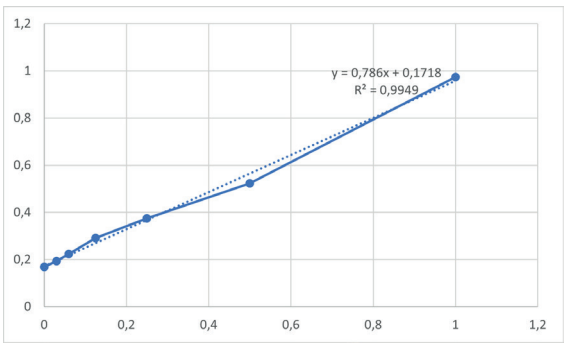

Figure 2. Gallic acid calibration curve

4. CONCLUSION

As far as we know when the literature was reviewed, the antioxidant effect of *S. lanata* has not been reported before. Our study, *S. lanata* with DPPH· scavenging activity method, can be considered the first report in terms of antioxidant activity. *S. lanata* extracts prepared with 70% ethanol were found to have higher DPPH· radical scavenging activity (0.241 mg/mL) than extracts prepared with other solvents, and according to the total phenolic method results, it was determined that the highest total phenol content was in the ethanolic (61.1±0.03 mg GAE/g) extract. The results confirmed a correlation between total phenol amount and antioxidant activity, as stated in many studies. In addition, in our study, the antibacterial effect was studied by selecting different strains from other antimicrobial activity experiments. It is very important to show the biological capacities of extracts. Therefore, in this study, *S. lanata* extracts were investigated for their advantages using various *in vitro* methods. With the successful demonstration of *in vivo* activity in future studies, a pharmaceutical product obtained from *S. lanata* will be safely functionalized.

Ethical approval

Not applicable, because this article does not contain any studies with human or animal subjects.

Author contribution

Concept: ZG, NS; Design: ZG; Supervision: YBK, Gİ; Materials: YBK; Data Collection and/or Processing: ZG, NS, Gİ, MK, YBK; Analysis and/or Interpretation: ZG, NS, Gİ, MK, YBK; Literature Search: ZG, NS; Writing: ZG, NS, Gİ, MK, YBK; Critical Reviews: Gİ, MK, YBK.

Source of funding

This research received no grant from any funding agency/sector.

Conflict of interest

The authors declared that there is no conflict of interest.

REFERENCES

1. Türkiye Bitkiler Listesi. Available at: https://www.bizimbitkiler.org.tr/v2/index.php
2. Çarıkçı S, Kılıç T, Azizoğlu A, Gülaçtı T. Chemical constituents of two endemic sideritis species from Turkey with antioxidant activity. Record of Natural Products. 2012;6(2):101-109.
3. González-Burgos E, Carretero ME, Gómez-Serranillos MP. Sideritis spp.: uses, chemical composition and pharmacological activities-a review. J Ethnopharmacol. 2011;135(2):209-225. https://doi.org/10.1016/j.jep.2011.03.014
4. Güner A, Aslan S, Ekim T, Vural M, Babaç MT (eds). Türkiye Bitkileri Listesi (Damarlı Bitkiler). İstanbul: Nezahat Gökyiğit Botanik Bahçesi ve Flora Araştırmaları Derneği Yayını; 2012.
5. Kirimer N, Tabanca N, Özek T, Tümen G, Baser KHC. Essential oils of annual sideritis species growing in Turkey. Pharm Biol. 2000;38(2):106-111. https://doi.org/10.1076/1388-0209(200004)3821-1FT106
6. Alipieva KI, Kostadinova EP, Evstatieva LN, Stefova M, Bankova VS. An iridoid and a flavonoid from Sideritis lanata L. Fitoterapia. 2009;80(1):51-53. https://doi.org/10.1016/j.fitote.2008.09.011
7. Ugur A, Varol O, Ceylan O. Antibacterial Activity of Sideritis curvidens and Sideritis lanata from Turkey. Pharmaceutical Biology. 2005;43(1):47-52. https://doi.org/10.1080/13880200590903354
8. Adams RP. Identification of Essential Oil Components by Gas Chromatography/Mass Spectrometry. Carol Stream, IL: Allured Publishing Corporation; 2007.
9. Hochmuth DH. MassFinder-4. Hamburg, Germany: Hochmuth Scientific Consulting; 2008.
10. McLafferty FW, Stauffer DB. The Wiley/NBS Registry of Mass Spectral Data. New York: J. Wiley and Sons; 1989.
11. Curvers J, Rijks J, Cramers C, Knauss K, Larson P. Temperature programmed retention indexes: calculation from isothermal data. Part 1: Theory. J High Resolut Chromatogr. 1985;8(9):607-610. https://doi.org/10.1002/jhrc.1240080926
12. Kumarasamy Y, Byres M, Cox PJ, Jaspars M, Nahar L, Sarker SD. Screening seeds of some Scottish plants for free radical scavenging activity. Phytother Res. 2007;21(7):615-621. https://doi.org/10.1002/ptr.2129
13. Singleton VL, Orthofer R, Lamuela-Raventós RM. Analysis of total phenols and other oxidation substrates and antioxidants by means of folinciocalteu reagent. Methods in Enzymology. 1999;299:152-178. https://doi.org/10.1016/S0076-6879(99)99017-1
14. Koşar M, Göger F, Can Başer KH. In vitro antioxidant properties and phenolic composition of Salvia virgata Jacq. from Turkey. J Agric Food Chem. 2008;56(7):2369-2374. https://doi.org/10.1021/jf073516b
15. Koutsaviti A, Bazos I, Milenković M, Pavlović-Drobac M, Tzakou O. Antimicrobial activity and essential oil composition of five Sideritis taxa of Empedoclia and Hesiodia Sect. from Greece. Records of Natural Products. 2013;7(1):6-14.
16. Stanoeva JP, Stefova M, Stefkov G, et al. Chemotaxonomic contribution to the Sideritis species dilemma on the Balkans. Biochemical Systematics and Ecology. 2015;61:477-487. https://doi.org/10.1016/j.bse.2015.07.008
17. Kirici D, Saltan N, Goger F, Kose YB, Demirci B. Chemical compositions of Sideritis albiflora Hub. - Mor. İstanbul Journal of Pharmacy. 2021;51(3):378-385. https://doi.org/10.26650/IstanbulJPharm.2021.908035
18. Koleva II, Linssen JPH, van Beek TA, Evstatieva LN, Kortenska V, Handjieva N. Antioxidant activity screening of extracts from Sideritis species (Labiatae) grown in Bulgaria. Journal of the Science of Food and Agriculture. 2003;83:809-819. https://doi.org/10.1002/jsfa.1415
19. Güvenç A, Houghton PJ, Duman H, Coşkun M, Şahin P. Antioxidant activity studies on selected sideritis species native to Turkey. Pharmaceutical Biology. 2005;43(2):173-177. https://doi.org/10.1080/13880200590919528

ANADOLU UNIVERSITY
INSTITUTE OF HEALTH SCIENCES

European Journal of Life Sciences 2022; 1: 70-88

Review Article

Release kinetics of 3D printed oral solid dosage forms: An overview

Berna Kaval[1,2], Engin Kapkın[3], Mustafa Sinan Kaynak[1,4]✉

[1]Anadolu University, Faculty of Pharmacy, Department of Pharmaceutical Technology, Eskisehir, Turkey.

[2]Mugla Sıtkı Kocman University, Koycegiz Vocational School of Health Services, Department of Pharmacy Services, Mugla, Turkey.

[3]Eskisehir Technical University, Faculty of Architecture and Design, Industrial Design Department, Eskişehir, Turkey.

[4]Anadolu University, Yunus Emre Vocational School of Health Services, Department of Pharmacy Services, Eskisehir, Turkey.

✉ Mustafa Sinan Kaynak
msk@anadolu.edu.tr

https://doi.org/10.55971/EJLS.1181158

Received: 28.09.2022
Accepted: 21.10.2022
Available online: 14.11.2022

ABSTRACT

Three-dimensional printing (3DP) is one of the most extensively researched methods for producing nano/micro scale biomaterials. This method is typically applied layer by layer. The 3DP method has many advantages over traditional manufacturing methods and ensures that personalized drug design is feasible. Individual dose adjustment provides significant benefits, particularly in some disadvantaged patient groups. Individual release characteristics may be required in these patient groups in addition to dose adjustment. 3DP technology also allows for the adjustment of release kinetics. All of these factors were also increasing interest in 3DP technology in the pharmaceutical industry. The goal of this review is to understand the pharmacological significance of 3DP technology as well as the parameters influencing the release profiles in tablets produced by using technique, and to establish a correlation between them. Within the scope of this review, 79 literature research studies were examined, and it was determined that there is limited data to determine whether there is a correlation between release kinetics and 3DP techniques. When the release profiles obtained by considering the polymer type used in these techniques are evaluated, immediate and rapid release was obtained in studies using PVA + PLA polymers and studies using PVP polymer, immediate release in studies using Kollidon® and Kollicoat® derivatives, and controlled, extended and sustained release was observed in studies using PCL polymer.

Keywords: 3D Printing, Personalized medicine, Release kinetic, Tablet design, Kinetic release model

1. INTRODUCTION

Depending on many factors, the therapeutic efficacy of medications varies. These considerations include drug release profiles, delivery mechanisms, and drug interactions within the body with the external environment. The release profile of drugs can be modified by the use of nano-and micro-size drug carriers in the formulation, such as biodegradable polymers, hydrogels, lipids, and even biological materials (eg, RNA and DNA) [1].

A lot of research has been published in recent years on the controlled release of important therapeutic drugs [2-5]. Researchers have developed many different methods to achieve the desired release of drugs and transport activity inside the body. Some of these methods include modifying the surface properties

of drug particles [6], attaching functional groups to the drug molecule to improve the interactions of drug particles with targeted cells or tissues [7], and extending the half-life of the drug in the body to trick the immune system by coating the drug with special polymers (e.g. polyethylene glycol or PEG). It remains an expensive and difficult method to change these drug molecules (i.e. size, shape, and surface characteristics) [1].

Three-dimensional (3D) printing consists of combining suitable materials to create a 3D object using a series of processes. Generally, this method is done layer by layer [8,9]. In another definition, 3D printing (3DP) refers to any process in which, by fusing layers on top of the material, 3D objects are created in a two-dimensional environment. In this process, a computer is required because 3DP is based on a "Computer-Aided Design" [10-12]. 3DP is also known as 'Additive Manufacturing' (AM). The ISO/ASTM standards describe the process of combining materials produced by layering using 3D model data in contrast to the formative and subtractive production methods [13,14].

The common point of all 3DP techniques called AM is their step-by-step or sequential processing. Compared to previous conventional methods, the manufacturing process based on 3DP techniques has significant advantages and disadvantages. In comparison to traditional methods, **Table 1** discusses some of the advantages and disadvantages of 3DP [8].

The purpose of this review is to understand the pharmacological significance of 3DP technology and one of the most common oral dosage forms obtained using these techniques, the parameters affecting release profiles in tablets.

2. 3D PRINTING TECHNOLOGY

3DP is one of the most studied methods of nano/microscale biomaterial processing. 3DP helps to make a lot of changes to the application scale. Although 3DP technology has shown considerable interest in tissue engineering, implants, and prosthetics, it is also very useful in the micro-manufacturing of drug particles. In addition to minimizing processing time, reducing costs, and being readily available, 3DP often provides high resolution at the stage of drug design [1,15].

New materials are evolving with the use of new applications, and 3DP methods are changing daily. With 3DP, it is possible to significantly minimize or fully eradicate the usage of various machines and facilities. In addition, it only allows custom designs by modifying the 3D model in the program, which during the prototyping process reduces the expense [8].

Table 1. Some advantages and disadvantages of 3DP vs Conventional Manufacturing

Advantages	Disadvantages	Ref.
There is no need for costly machinery for metal smelting plants and for milling pro-cesses	The capacity to generate at low num-bers and speeds	[90]
The ability to create components in a short time with complicated and personalized unconventional structures	Lower surface gloss, accuracy and strength	[91]
The less eco-friendly waste generation and recycling process is	The comparatively few materials that can be processed and reflect the kind of production products	[92]
Cost-effective for low volume and small batch production	The broad restriction on structural di-mensions	[93]

Traditional tablet manufacturing process; current technologies require a variety of unit operations, such as mixing, milling, granulation, drying, compression. In addition, it is necessary to have some costly equipment/tools that require experienced personnel, take a long time and require invest money. All of these make commercially available oral dosage formulations to be costly for the consumer [16]. Apart from these, amid all of these investments, there are so many deficiencies in the production of customized medicines with technologies currently available [17,18].

By allowing individual drugs to be precisely designed, 3DP technology will fill this void. Previous research experiments have shown that to personalize drugs, 3DP can be used [19].

With 3DP technology, which is one of the pharmaceutical technologies through which specific changes can be made, it is unavoidable that doses of the medication's active ingredients should be prepared individually. Dose personalization is not needed for a lot of drugs. But in some other patient groups, in children and particularly in therapies where medications with high toxicity and a limited therapeutic window are used, the individual dose adjustments can offer significant benefits [20]. In addition, the dosage requirements for neonatal, pediatric, and geriatric patients differ considerably from adult dose [21]. In addition, patients with organ dysfunction can need a dosage change to prevent drug toxicity. Although the techniques available in pharmaceutical manufacturing are useful for mass production, 3DP allows for customized, small-scale production. The dosage quantity, geometry, and even the drug release profile can be easily met after customization using 3DP, in line with all these needs. It will also play a vital role in the practice of precision medicine [20,21].

With the approval of Spritam® (levetiracetam), developed using 3DP technology in 2015, by the FDA (U.S. Food and Drug Administration), the use of this technology in the pharmaceutical industry was officially approved for the first time. Spritam®, an anti-epileptic drug developed by Aprecia Pharmaceuticals, is dispersed in the mouth with a very small amount of water in less than 10 seconds, making it very easy to use in the population of disadvantaged patients (eg. pediatric patients, elderly patients) [19-22].

3. 3D PRINTING TECHNIQUES

Inside 3DP technology, there are different approaches. It is possible to group the 3DP methods under five major headings. These include:

- Vat Polymerization,
- Powder Bed Fusion,
- Material Extrusion,
- Material Jetting,
- Direct Energy Deposition.

There are various techniques under each heading. The materials used are different and limited due to the various processes used in 3DP technology used for various purposes. Therefore, only some of them can be utilized in pharmaceutical production [21-23]. In this title, only the techniques that can be used in pharmaceutical applications will be mentioned and detailed.

3.1. Vat Polymerization

The final product of the vat polymerization technique; is obtained by initiating chain reactions in the starting product through various means (UV-light, radiation, electron beam, etc.). Stereolithography (SLA), Digital Light Processing (DLP), 2-Photon Polymerization (2-PP), and Continuous Liquid

Interface Production (CLIP) techniques will be discussed in this section, which comes under the category of vat polymerization and can be used for drug production [21-23].

3.1.1. Stereolithography (SLA)

One of 3DP's key methods, developed in 1986, is SLA [12,24]. In this procedure, by sending UV-light (or electron beams) to a resin layer or a monomer solution, a chain reaction is initiated. By transforming UV-light into a radical form, the monomers used (mainly epoxy-based or acrylic-based) become active. These activated monomers are converted into polymers instantly [8,25]. The resin that is treated with UV light solidifies after polymerization. The remaining component is extracted from the environment using several processes when the printing process is completed [26].

3.1.2. Digital Light Processing (DLP)

This technique is carried out using a photopolymer such as SLA. The difference between these two methods is that the sources of radiation used are distinct. It is a quicker method than the SLA technology [8,27].

3.1.3. 2-Photon Polymerization (2-PP)

2-PP is also referred to as Multiphoton Polymerization. Higher resolution than the SLA system. It is a process that works by polymerizing photo-sensitive material due to the absorption of photons at or above 780-820 nm wavelength and enables micro-and nano-sized printing [8,10,28].

3.1.4. Continuous Liquid Interface Production (CLIP)

It was developed as a new technology for 3DP in 2015. 3D printed models constructed in 2-dimensions are made possible by sending UV-light to liquid resin in the transparent window region. This method based on the photopolymerization process has allowed printing speed and resolution to be improved [29].

3.2. Powder Bed Fusion

The product is obtained after operations on the powder mass, which consists of solid-micro-sized particles on a plane, in the Powder Bed Fusion technique. This section will go over the Selective Laser Sintering (SLS) technique, which is part of the Powder bed fusion technique and can be used for drug production [21,23].

3.2.1. Selective Laser Sintering (SLS)

The most widely used industrial 3DP method is SLS [30,31]. When putting together micro-sized particles in a powder bed to create the finished product, SLS is applied using laser light. In this method [32-35], several different materials, including metals and different thermoplastic materials, are used. In particular, the method enables products with complex geometries to be created [30].

3.3. Material Extrusion

The starting product in the Material Extrusion technique can be semi-solid or solid. This starting product is extruded to produce the final product. This section will go over Fused Deposition Modeling (FDM) and the Pneumatic Extraction / Syringe Extrusion (PE / SE) technique, which can also be used for Material drug production [21,23].

3.3.1. Fused Deposition Modelling (FDM)

The FDM process is based on the thermoplastic polymer's layer-by-layer fusion and solidification by heating to make it semi-solid [12,36,37]. Some

of the advantages are the speed, low cost, and easy processing required by the system [38].

3.3.2. Pneumatic Extrusion / Syringe Extrusion (PE / SE)

For the printing of different semi-solid formulations, such as hydrogels and pastes, the PE / SE method has been developed. A temperature control unit on the syringe system may also control the temperature of the printing material. The temperature regulation of the printing material helps to regulate the material's viscosity and to maintain the material in a semi-solid state that enables the material to be 3D printed [39].

3.4. Material Jetting

In the material jetting technique, it is obtained after the starting product is cured after spraying directly on the surface or after the bonding agent is sprayed on the starting product. Under the main heading of Material Jetting technique, this section will discuss the Material Jetting (MJ) and Binder Jetting (BJ) techniques [21,23].

3.4.1. Material Jetting (MJ)

Among 3DP technologies, MJ allows hard and soft polymer products to be processed in a single process in different colors, with different materials [40]. The material jet allows the modification of the material properties [41]. The photosensitive polymer resin coating is sprayed on the surface by the material jet printer, which releases UV-light into the environment, resulting in the final product [42].

3.4.2. Binder Jetting (BJ)

BJ, one of the 3DP techniques, is based on the concept of spraying a binder solution onto a powder bed [43-45]. The binder solution used in this process must have certain properties. As the average molecular weight and polymer concentration of the solution increase, the viscosity of the binding solution increases, and the substance cannot be printed [46].

4. RELEASE KINETICS AND INFLUENCING PARAMETERS

There are a lot of parameters that affect the kinetics of release. Changing the shape of the particles of the drug first impacts the particles' surface area, causing many changes in their properties [47,48]. If the particle's surface area increases, the particles' size decreases. Reducing the size of the particle increases the particle's surface area and solubility, respectively. It can also be used to improve drug solubility as a safe method [48-51]. Considering the effect on the solubility of the change in particle size, it can be predicted that the change in particle surface area will also have a significant impact on solubility [1].

The drug release profile can also be affected by modifying the 3D shape/structure of the drug particle. A change in the shape of the particle, as mentioned earlier, may cause a change in the surface area that changes the solubility of the drug and as a consequence, changes the kinetics of the release of the drug [52]. As a consequence, a major factor that affects the surface area, drug release kinetics, and therefore its interaction with tissue and cell, is the shift in the particle shape/structure of drugs [1].

Kinetic models used in drug release research have an important role to play in assessing drug release mechanisms. A variety of clinical models have been adopted to specifically define and address the mechanism for the release of drugs for various drugs [53-55]. These clinical models and equations are shown in **Table 2.**

Table 2. Kinetic release model equations.

Model	Equation	Parameters
Zero order	$Q = Q_0 + K_0 t$	K_0 −zero order release constant
First-order	$\frac{dC}{dt} = -K_1 C$	K_1 −first-order release constant C–drug concentration
Higuchi	$Q = K_H t^{0.5}$	K_H–Higuchi constant
Korsmeyer-Peppas	$\frac{Q_t}{Q_\infty} = K_{KP}.t^n$	K_{KP} −constant with structural and geometric information n–indicative release mechanism
Peppas-Sahlin	$Q = K_1.t^m + K_2.t^{2m}$	K_1 −constant indicating Fickian diffusion contribution K_2 −constant indicating case II transport contribution m −purely Fickian diffusion exponent
Weibull	$\log\left[-\ln\left(1-\frac{Q_t}{Q_\infty}\right)\right] = \beta.\log t - \log\alpha$	α −scale parameter β −shape parameter
Hopfenberg	$\frac{Q_t}{Q_\infty} = 1 - \left[1 - \frac{K_{HB}.t}{C_0.a_0}\right]^n$	K_{HB} −erosion rate constant C_0 −initial drug concentration in matrix a_0 −initial radius of the form n −geometry dependent exponent (n=2 for cylindrical forms)
Hixson-Crowell	$Q_0^{1/3} - Q_t^{1/3} = K_{HC}t$	K_{HC} −constant dependent on the surface-volume relation

Q_0 −initial amount of drug in dosage form, Q_t −amount of drug dissolved in time, Q_∞ −total dissolved drug amount when dosage form exhausted, $^{Q_t}/_{Q_\infty}$ −fraction drug dissolved [54, 55, 72].

5. RELEASE KINETICS ON 3D PRINTED ORAL DOSAGE FORMS

In the studies performed, many different 3DP technologies have been used to produce pharmaceutical dosage forms [56-60]. Using these 3DP methods, parameters such as size, geometry, and surface area of the dosage form may be altered [61-63]. These interventions have made it easy to improve the release properties of the drug. In addition, studies have increased the solubility of active pharmaceutical ingredients with low solubility properties using 3DP technology [64-66]. Interest in the use of 3DP techniques in the pharmaceutical industry is increasing every day due to their unique capabilities [67,68].

Because tablets, which are the most commonly used solid dosage type in the pharmaceutical industry, are easy to use by the consumer, patient compliance is high and their production is cheaper than other dosage forms, it is observed that the studies were mainly based on tablets [19,69,70].

The comparison of oral dosage forms obtained using 3DP technology for various parameters in this compilation analysis is shown in **Table 3**.

Table 3. Comparison in terms of various parameters of oral dosage forms developed using 3DP Technologies

Active Pharmaceutical Ingredient	Dosage Form	Release Profile	Release Kinetic Model	3DP Technique	Polymer	Ref.
4-Aminosalicylic acid	Tablet	Immediate release	N/A	FDM	Kollidon® 12 PF	[80]
Ramipril					Kollidon® VA 64	
4-Aminosalicylic acid	Tablet	Modified release	N/A	FDM	PVA filament	[94]
5-Aminosalicylic acid						
5-Fluorouracil	Patch	Prolonged release	N/A	Syringe extrusion	PLGA	[95]
		Controlled release			PCL	
Amitriptyline HCl	Tablet	Immediate release	N/A	Binder jetting	PVP	[19]
Ascorbic acid	Hydrogel	Controlled Release	N/A	SLA	Poly(ethylene glycol) dimethacrylate	[96]
Aspirin	Tablet	Sustained Release	N/A	SLA	PCL	[97]
Paracetamol					PEGDA	
Aspirin	Tablet	Immediate release	N/A	Syringe extrusion	HPMC	[58]
Atenolol						
Hydrochlorothiazide						
Pravastatin		Sustained release				
Ramipril						
Bicalutamide	Tablet	Combined release (Immediate release and Controlled release)	N/A	FDM	Kollicoat® IR	[81]
					PLA	
					PLA filament	
					PVA filament	
Budesonide	Tablet	Controlled release	N/A	FDM	PVA filament	[98]
		Modified release				
Caffeine	Tablet	N/A	Higuchi	Binder jetting	HPC	[20]
Caffeine	Caplet (DuoCaplet)	Delayed release	N/A	FDM	PVA filament	[15]
Paracetamol		Controlled release				
Calcein	Tablet	Controlled release	N/A	FDM	PVA	[99]
Fluorescein					PLA Filament	
Captopril	Tablet	Rapidly dispersing	N/A	Binder jetting	Mannitol	[87]
Captopril	Tablet	Sustained release	First-order	Syringe extrusion	Cellulose acetate	[71]
Glipizide			Korsmeyer–Pappas		HPMC	
Nifedipin						
Carbamazepine	Scaffold	Sustained release	Zero order	FDM	ABS filament	[100]
Carvedilol	Tablet	Rapid release	N/A	Material jetting	PEGDA	[78]
					PVP	

Table 3. Continued

Active Pharmaceutical Ingredient	Dosage Form	Release Profile	Release Kinetic Model	3DP Technique	Polymer	Ref.
Carvedilol	Tablet	Extended release	Hopfenberg Korsmeyer-Peppas Peppas-Sahlin	FDM	Affinisol™ HPMC HME 15LV Eudragit® E PO HPC HPMC Kollidon® SR	[72]
Catechin	Muco-Adhesive Oral Films	Controlled release	N/A	Syringe extrusion	HPMC	[101]
Cefazolin	Scaffold	Sustained release	N/A	FDM	PCL Gelatin methacrylate	[82]
Cidofovir	Bioadhesive film	Modified release	N/A	Binder jetting	PEG-PCL	[83]
Paclitaxel		Controlled release			PCL	
Ciprofloxacin HCl	Tablet	N/A	Zero order	FDM	PVA	[75]
Copper sulphate (II) pentahydrate Silver nitrate Zinc oxide	Wound dressings (nose and ear)	Controlled release	N/A	FDM	PCL	[84]
Curcumin	Tablet	Controlled release	N/A	FDM	PVA filament	[102]
Deflazacort	Tablet	Prolonged release	N/A	FDM	PCL Eudragit® RL 100 Eudragit® RS 100	[103]
Dexamethasone	Scaffold	Controlled release	N/A	FDM	PCL Poloxamine (Tetronic®)	[104]
Dexamethasone-21-phosphate disodium salt	Scaffold	Prolonged release	N/A	Syringe extrusion	PLGA PVA	[105]
Dipyridamole	Tablet	Sustained release	N/A	Syringe extrusion	HPMC	[106]
Domperidone Ibuprofen	Suppository	N/A	N/A	FDM	PVA filament PEG 400 PEG 6000	[107]
Dronedarone HCl	Tablet	Controlled release	Hixson-Crowell	FDM	PEG PVA filament	[73]
Efavirenz Emtricitabine Tenofovir disoproxil fumarate	Tablet	Controlled release	N/A	Syringe extrusion	Hydroxyethylcellulose ethoxylate	[108]
Fenofibrate	Tablet	Controlled release Tuneable release	N/A	Syringe extrusion	Beeswax	[109]
Fibroblast growth factor-2	Scaffold	Sustained release	N/A	FDM	Calcium Silicate/PCL	[110]
Fluorescein	Tablet	N/A	N/A	FDM	PVA filament	[111]

Table 3. Continued

Active Pharmaceutical Ingredient	Dosage Form	Release Profile	Release Kinetic Model	3DP Technique	Polymer	Ref.
Gentamicin sulfate Methotrexate	Endovascular catheter	Sustained release	N/A	FDM	PLA	[112]
Ginkgolide	Tablet	Controlled release	N/A	Syringe extrusion	HPMC	[113]
Glimepiride Metformin	Tablet	Sustained release	N/A	FDM	PVA Eudragit® RL	[114]
Glipizide	Tablet	Controlled release	Korsmeyer–Peppas	FDM	PVA filament	[76]
Guaifenesin	Tablet	Sustained release	N/A	Syringe extrusion	HPMC Poly(acrylic acid)	[68]
Haloperidol	Tablet	Immediate release	N/A	FDM	Kollidon® VA 64 Kollicoat® IR Affinisol™HPMC HME 15 cP HPMCAS	[61]
Hydrochlorothiazide	Tablet	Immediate release	N/A	FDM	Eudragit® E	[63]
Ibuprofen Riboflavin	Tablet	Delayed release	N/A	SLA	PEGDA PEG 300	[115]
Ibuprofen Paracetamol	Fast-dissolving oral films	Extended release	N/A	FDM	PEO PVA PEG	[116]
Indomethacin	Tablet	N/A	N/A	FDM	PEG HPMCAS	[117]
Indomethacin	Implant	Controlled release	N/A	FDM	PCL	[118]
Indomethacin	Implant	N/A	Higuchi	FDM	Ethylene vinyl acetate	[119]
Insulin	Microneedle	Rapid release	N/A	SLA Binder jetting	Mannitol Xylitol Resin	[88]
Isoniazid Rifampicin B	Implant	Extended release	N/A	FDM	PLA Filament PEO PVA filament	[120]
Lamivudine	Capsule	Delayed release	N/A	FDM	PVA	[121]
Levofloxacin	Implant	Burst release Pulsed release	N/A	Binder jetting	PLA	[122]
Levofloxacin Rifampin Vancomycin	Scaffold	Prolonged release Sustained release	N/A	Syringe extrusion	Gelatin-Glutaraldehyde PVA	[123]
Metformin HCl	Tablet	N/A	N/A	FDM	PVA filament	[124]
Metformin HCl	Capsule	Tunable release	N/A	FDM	PLA Filament PVA filament	[125]
Metronidazole	Tablet	N/A	Zero order	FDM	PVA	[126]
Nitrofurantoin	Implant	Controlled release	N/A	FDM	PLA	[127]

Table 3. Continued

Active Pharmaceutical Ingredient	Dosage Form	Release Profile	Release Kinetic Model	3DP Technique	Polymer	Ref.
Ofloxacin Tetracycline Vancomycin	Implant	Sustained release	N/A	Binder jetting	Dicalcium phosphate anhydrous (monetite, CaHPO4) Hydroxyapatite Dicalcium phosphate dihydrate (brushite, CaHPO4·2H2O)),	[128]
Pantoprazole sodium	Tablet	Immediate release	N/A	FDM	PEG 6000 Kollidon® VA 64 Kollicoat® IR PEO 100,000 PVP Poloxamer 407 PEG 20000	[79]
Paracetamol	Tablet	Controlled release	Zero order First-order	FDM	HPC	[74]
Paracetamol	Tablet	Controlled release	N/A	FDM	PVA filament	[62]
Paracetamol	Tablet	Controlled release	N/A	FDM	HPMC	[129]
Paracetamol	Tablet	Controlled release	N/A	FDM	EC Eudragit® L 100 HPC HPMC Soluplus®	[130]
Paracetamol	Tablet	Controlled release	N/A	FDM	HPMCAS	[131]
Paracetamol	Tablet	Immediate release Modified release	N/A	SLS	Kollicoat® IR Eudragit® L 100 EC	[132]
Prednisolone	Tablet	Extended release	N/A	FDM	PVA filament	[17]
Prednisolone	Implant	Controlled release	N/A	Syringe extrusion	Polydimethylsiloxane	[133]
Progesterone	Biodegradable projectile	Extended release	N/A	FDM	PLA	[134]
Progesterone	Implant	Controlled release	N/A	FDM	PCL PLA	[85]
Propranolol HCl	Orodispersible drug delivery systems	Immediate release	N/A	Binder jetting	HPC	[135]
Propranolol HCl (Indicardin®, 40 mg)	Tablet	Controlled release	N/A	FDM	Cellulose acetate D-Mannitol PEG 6000	[89]

Table 3. Continued

Active Pharmaceutical Ingredient	Dosage Form	Release Profile	Release Kinetic Model	3DP Technique	Polymer	Ref.
Rasagiline mesylate	Orodispersible films / Transparency films	Prolonged release	N/A	Binder jetting	HPMC / Crospovidone	[136]
rhBMP2 (recombined human bone morphogenetic protein-2)	Scaffold	Controlled release / Non-controlled release	N/A	Syringe extrusion	Chitosan	[137]
Riboflavin	Tablet	Controlled release	N/A	FDM	PLA Filament / PVA / PCL	[138]
Rodhamine B	Hydrogel Patches	Controlled release	N/A	Syringe extrusion	Alginic acid sodium salt / Starch	[139]
Ropinirole HCl	Tablet	N/A	Korsmeyer-Peppas	Material jetting	PEGDA	[59]
Salicylic acid	Patches (nose-shape)	N/A	N/A	FDM / SLA	PLA filament / PCL Filament / PEGDA / PEG	[86]
Theophylline	Tablet	Sustained release	Korsmeyer-Peppas	FDM	Eudragit® FS 30 D / HPMC / PLA filament	[77]
Theophylline	Tablet	Extended release	N/A	Syringe extrusion	HPMC	[140]
Thiamine HCl	Tablet	Rapid release	N/A	Binder jetting	PVP	[56]
Vancomycin	Bone graft	N/A	N/A	Syringe extrusion	Sodium alginate	[141]
Warfarin	Tablet	Immediate release	N/A	FDM	Eudragit® E PO	[142]

*N/A: Not Available
**ABS: Acrylonitrile butadiene styrene, EC: Ethylcellulose, HPC: Hydroxypropyl cellulose, HPMC: Hydroxypropyl methylcellulose, HPMCAS: Hydroxypropyl methylcellulose acetate succinate, PCL: Poly-ε-caprolactone, PEG: Polyethylene glycol, PEGDA: Poly(ethylene glycol) diacrylate, PEO: Poly(ethylene oxide), PLA: Polylactic acid, PVA: Polyvinyl alcohol, PVP: Polyvinyl pyrrolidone

6. RESULTS

This review research examined 79 publications in total. When the studies using the release kinetic models in **Table 4** were examined, there was no correlation between the polymer type or print technique and the release kinetic model. Only 15.19% of the 79 studies included release kinetics studies. The kinetics of the active substance's release from the dosage form was not determined in the studies under review, which is believed to be one of the reasons why no correlation could be found.

When the results of the investigations are considered together, no conclusion can be drawn that single release kinetics was obtained in studies using Eudragit® derivatives, PEG, PEGDA, or Cellulose-derived polymers [20,71-74]. However, in research studies PVA and PLA polymers, immediate or rapid release was obtained [73,75-77]. In studies involving PVP polymer, it was found that immediate and rapid release was obtained [19,56,78,79]. Other than Kollidon® SR, the immediate release was observed in studies using Kollidon® and Kollicoat® derivatives [61,72,79-81]. PCL polymer, which provides longer

Table 4. Release kinetic models calculated in studies

3DP Technique	Release Kinetic Model	Polymer	Ref.
Binder jetting	Higuchi	HPC	[20]
FDM	Zero order	ABS filament	[100]
	Hopfenberg	Affinisol™ HPMC HME 15LV	[72]
		Eudragit® E PO	
	Korsmeyer-Peppas	HPC	
		HPMC	
	Peppas-Sahlin	Kollidon® SR	
	Zero order	PVA	[75]
	Hixson-Crowell	PEG	[73]
		PVA filament	
	Korsmeyer-Peppas	PVA filament	[76]
	Higuchi	Ethylene vinyl acetate	[119]
	Zero order	PVA	[126]
	Zero order	HPC	[74]
	First-order		
	Korsmeyer-Peppas	Eudragit® FS 30 D	[77]
		HPMC	
		PLA filament	
Material jetting	Korsmeyer-Peppas	PEGDA	[59]
Syringe extrusion	First-order	Cellulose acetate	[71]
	Korsmeyer-Pappas	HPMC	

*ABS: Acrylonitrile butadiene styrene, HPC: Hydroxypropyl cellulose, HPMC: Hydroxypropyl methylcellulose, PEG: Polyethylene glycol, PEGDA: Poly(ethylene glycol) diacrylate, PVA: Polyvinyl alcohol.

drug release, has been used to achieve prolonged release, controlled release, and sustained release [82-86]. Except for one study, the rapid release was obtained in mannitol studies [87,88]. Mannitol was used in combination with cellulose acetate and PEG in the study, which resulted in controlled release rather than a rapid release [89].

7. CONCLUSION

This study demonstrates the methods, active pharmaceutical agents, polymers, pharmaceutical dosage formulations, and release kinetics used in 79 studies and trials. This research, which we have done, illustrates clearly the benefits of using 3DP techniques in the pharmaceutical industry. It would be very convenient to use it in the development of personalized drugs in the future, considering the advantages of 3DP technologies, such as the ability to modify the dose, to alter the geometry of the dosage shape, to adjust the surface area, to be cheaper and simpler than traditional methods. This is a very convenient technology, especially for vulnerable patients, such as the elderly and children, for the production of drugs at sensitive doses. The parameters needed for production will be better understood and more controllable as the research performed with 3DP technologies increases. Future studies should also establish and define GMP (Good Manufacturing Practice) and QbD (Quality by Design) procedures. The predicted outcome in the future would be that 3DP technology will be used by the pharmaceutical industry and that more approved products will be developed on the market using 3DP technology.

Author contribution

Concept: MSK, EK; Design: MSK, EK; Supervision: MSK; Materials: BK; Data Collection and/or Processing: BK; Analysis and/or Interpretation: BK, MSK, EK; Literature Search: BK; Writing: BK; Critical Reviews: MSK, EK.

Source of funding

This research received no grant from any funding agency/sector.

Conflict of interest

The authors declared that there is no conflict of interest.

REFERENCES

1. Curry EJ, Henoun AD, Miller AN 3rd, Nguyen TD. 3D nano- and micro-patterning of biomaterials for controlled drug delivery. Ther Deliv. 2017;8(1):15-28. https://doi.org/10.4155/tde-2016-0052
2. Lavan DA, McGuire T, Langer R. Small-scale systems for in vivo drug delivery. Nat Biotechnol. 2003;21(10):1184-1191. https://doi.org/10.1038/nbt876
3. Prausnitz MR, Mitragotri S, Langer R. Current status and future potential of transdermal drug delivery. Nat Rev Drug Discov. 2004;3(2):115-124. https://doi.org/10.1038/nrd1304
4. Kaynak MS, Kaş HS, Levent Ö. Formulation of controlled release glipizide pellets using pan coating method. Hacettepe University Journal of the Faculty of Pharmacy. 2007;27(2):93-106.
5. Langer R. New methods of drug delivery. Science. 1990;249(4976):1527-1533. https://doi.org/10.1126/science.2218494
6. Liversidge GG, Cundy KC, Bishop JF, Czekai DA, inventors; Particulate Prospects Corp, Elan Corp PLC, Elan Pharma International Ltd, assignee. Surface modified drug nanoparticles. United States patent DC 5,145,684. 1992.
7. Fang C, Bhattarai N, Sun C, Zhang M. Functionalized nanoparticles with long-term stability in biological media. Small. 2009;5(14):1637-1641. https://doi.org/10.1002/smll.200801647
8. Kholgh Eshkalak S, Rezvani Ghomi E, Dai Y, Choudhury D, Ramakrishna S. The role of three-dimensional printing in healthcare and medicine. Materials & Design. 2020;194:108940. https://doi.org/10.1016/j.matdes.2020.108940
9. Basgul C, Yu T, MacDonald DW, Siskey R, Marcolongo M, Kurtz SM. Structure-Property Relationships for 3D printed PEEK Intervertebral Lumbar Cages Produced using Fused Filament Fabrication. J Mater Res. 2018;33(14):2040-2051. https://doi.org/10.1557/jmr.2018.178
10. Ligon SC, Liska R, Stampfl J, Gurr M, Mülhaupt R. Polymers for 3D Printing and Customized Additive Manufacturing. Chem Rev. 2017;117(15):10212-10290. https://doi.org/10.1021/acs.chemrev.7b00074
11. Kjar A, Huang Y. Application of Micro-Scale 3D Printing in Pharmaceutics. Pharmaceutics. 2019;11(8):390. https://doi.org/10.3390/pharmaceutics11080390
12. Ngo TD, Kashani A, Imbalzano G, Nguyen KTQ, Hui D. Additive manufacturing (3D printing): A review of materials, methods, applications and challenges. Composites Part B: Engineering. 2018;143:172-196. https://doi.org/10.1016/j.compositesb.2018.02.012
13. Dizon JRC, Espera AH Jr, Chen Q, Advincula RC. Mechanical characterization of 3D-printed polymers. Additive Manufacturing. 2018;20:44-67. https://doi.org/10.1016/j.addma.2017.12.002
14. Honigmann P, Sharma N, Okolo B, Popp U, Msallem B, Thieringer FM. Patient-Specific Surgical Implants Made of 3D Printed PEEK: Material, Technology, and Scope of Surgical Application. Biomed Res Int. 2018;2018:4520636. https://doi.org/10.1155/2018/4520636
15. Goyanes A, Wang J, Buanz A, et al. 3D Printing of Medicines: Engineering Novel Oral Devices with Unique Design and Drug Release Characteristics. Mol Pharm. 2015;12(11):4077-4084. https://doi.org/10.1021/acs.molpharmaceut.5b00510
16. Scoutaris N, Alexander MR, Gellert PR, Roberts CJ. Inkjet printing as a novel medicine formulation technique. J Control Release. 2011;156(2):179-185. https://doi.org/10.1016/j.jconrel.2011.07.033
17. Skowyra J, Pietrzak K, Alhnan MA. Fabrication of extended-release patient-tailored prednisolone tablets via fused deposition modelling (FDM) 3D printing. Eur J Pharm Sci. 2015;68:11-17. https://doi.org/10.1016/j.ejps.2014.11.009
18. Tutton R. Personalizing medicine: futures present and past. Soc Sci Med. 2012;75(10):1721-1728. https://doi.org/10.1016/j.socscimed.2012.07.031

19. Sen K, Manchanda A, Mehta T, Ma AWK, Chaudhuri B. Formulation design for inkjet-based 3D printed tablets. Int J Pharm. 2020;584:119430. https://doi.org/10.1016/j.ijpharm.2020.119430

20. Infanger S, Haemmerli A, Iliev S, Baier A, Stoyanov E, Quodbach J. Powder bed 3D-printing of highly loaded drug delivery devices with hydroxypropyl cellulose as solid binder. Int J Pharm. 2019;555:198-206. https://doi.org/10.1016/j.ijpharm.2018.11.048

21. Khan FA, Narasimhan K, Swathi CSV, et al. 3D Printing Technology in Customized Drug Delivery System: Current State of the Art, Prospective and the Challenges. Curr Pharm Des. 2018;24(42):5049-5061. https://doi.org/10.2174/1381612825666190110153742

22. Jamroz W, Kurek M, Lyszczarz E, Brniak W, Jachowicz R. Printing techniques: recent developments in pharmaceutical technology. Acta Pol Pharm. 2017;74(3):753-763.

23. Lim SH, Kathuria H, Tan JJY, Kang L. 3D printed drug delivery and testing systems - a passing fad or the future? Adv Drug Deliv Rev. 2018;132:139-168. https://doi.org/10.1016/j.addr.2018.05.006

24. Melchels FPW, Feijen J, Grijpma DW. A review on stereolithography and its applications in biomedical engineering. Biomaterials. 2010;31(24):6121-6130. https://doi.org/10.1016/j.biomaterials.2010.04.050

25. Devi L, Gaba P, Chopra H. Tailormade Drug Delivery System: A Novel Trio Concept of 3DP+ Hydrogel+ SLA. J Drug Delivery Ther. 2019;9(4-s):861-866. https://doi.org/10.22270/jddt.v9i4-s.3458

26. Zhou T, Zhang L, Yao Q, et al. SLA 3D printing of high quality spine shaped β-TCP bioceramics for the hard tissue repair applications. Ceramics International. 2020;46(6):7609-7614. https://doi.org/10.1016/j.ceramint.2019.11.261

27. Zhang J, Hu Q, Wang S, Tao J, Gou M. Digital Light Processing Based Three-dimensional Printing for Medical Applications. Int J Bioprint. 2019;6(1):242. https://doi.org/10.18063/ijb.v6i1.242

28. Chartrain NA, Williams CB, Whittington AR. A review on fabricating tissue scaffolds using vat photopolymerization. Acta Biomater. 2018;74:90-111. https://doi.org/10.1016/j.actbio.2018.05.010

29. Tumbleston JR, Shirvanyants D, Ermoshkin N, et al. Additive manufacturing. Continuous liquid interface production of 3D objects. Science. 2015;347(6228):1349-1352. https://doi.org/10.1126/science.aaa2397

30. Whitehead J, Lipson H. Inverted multi-material laser sintering. Additive Manufacturing. 2020;36:101440. https://doi.org/10.1016/j.addma.2020.101440

31. Anderson I. Mechanical properties of specimens 3D printed with virgin and recycled polylactic acid. 3D Printing and Additive Manufacturing. 2017;4(2):110-115. https://doi.org/10.1089/3dp.2016.0054

32. Bakshi KR, Mulay AV. A review on selective laser sintering: a rapid prototyping technology. IOSR. 2016;04(04):53-57. https://doi.org/10.9790/1684-15008040453-57

33. Kumar S. Selective laser sintering: a qualitative and objective approach. JOM. 2003;55(10):43-47. https://doi.org/10.1007/s11837-003-0175-y

34. Agarwala M, Bourell D, Beaman J, Marcus H, Barlow J. Direct selective laser sintering of metals. Rapid Prototyping Journal. 1995;1(1):26-36. https://doi.org/10.1108/13552549510078113

35. Kruth JP, Wang X, Laoui T, Froyen L. Lasers and materials in selective laser sintering. Assembly Automation. 2003;23(4):357-371. https://doi.org/10.1108/01445150310698652

36. Haryńska A, Kucinska-Lipka J, Sulowska A, Gubanska I, Kostrzewa M, Janik H. Medical-Grade PCL Based Polyurethane System for FDM 3D Printing-Characterization and Fabrication. Materials (Basel). 2019;12(6):887. https://doi.org/10.3390/ma12060887

37. Gnanasekaran K, Heijmans T, van Bennekom S, et al. 3D printing of CNT- and graphene-based conductive polymer nanocomposites by fused deposition modeling. Applied Materials Today. 2017;9:21-28. https://doi.org/10.1016/j.apmt.2017.04.003

38. Sood AK, Ohdar RK, Mahapatra SS. Parametric appraisal of mechanical property of fused deposition modelling processed parts. Materials & Design. 2010;31(1):287-295. https://doi.org/10.1016/j.matdes.2009.06.016

39. Panraksa P, Udomsom S, Rachtanapun P, Chittasupho C, Ruksiriwanich W, Jantrawut P. Hydroxypropyl Methylcellulose E15: A Hydrophilic Polymer for Fabrication of Orodispersible Film Using Syringe Extrusion 3D Printer. Polymers (Basel). 2020;12(11):2666. https://doi.org/10.3390/polym12112666

40. Loh GH, Pei E, Harrison D, Monzón MD. An overview of functionally graded additive manufacturing. Additive Manufacturing. 2018;23:34-44. https://doi.org/10.1016/j.addma.2018.06.023

41. Salcedo E, Baek D, Berndt A, Ryu JE. Simulation and validation of three dimension functionally graded materials by material jetting. Additive Manufacturing. 2018;22:351-359. https://doi.org/10.1016/j.addma.2018.05.027

42. Tee YL, Tran P, Leary M, Pille P, Brandt M. 3D Printing of polymer composites with material jetting: Mechanical and fractographic analysis. Additive Manufacturing. 2020;36:101558. https://doi.org/10.1016/j.addma.2020.101558

43. Prasad LK, Smyth H. 3D Printing technologies for drug delivery: a review. Drug Dev Ind Pharm. 2016;42(7):1019-1031. https://doi.org/10.3109/03639045.2015.1120743

44. Reis N, Ainsley C, Derby B. Ink-jet delivery of particle suspensions by piezoelectric droplet ejectors. Journal of Applied Physics. 2005;97(9):094903. https://doi.org/10.1063/1.1888026

45. Bai Y, Wagner G, Williams CB. Effect of particle size distribution on powder packing and sintering in binder jetting additive manufacturing of metals. Journal of Manufacturing Science and Engineering. 2017;139(8). https://doi.org/10.1115/1.4036640

46. Wilts EM, Long TE. Thiol-ene addition enables tailored synthesis of poly(2-oxazoline)-graft-poly(vinyl pyrrolidone) copolymers for binder jetting 3D printing. Polym Int. 2020;69(10):902-911. https://doi.org/10.1002/pi.6074

47. Champion JA, Katare YK, Mitragotri S. Particle shape: a new design parameter for micro- and nanoscale drug delivery carriers. J Control Release. 2007;121(1-2):3-9. https://doi.org/10.1016/j.jconrel.2007.03.022

48. Khadka P, Ro J, Kim H, et al. Pharmaceutical particle technologies: An approach to improve drug solubility, dissolution and bioavailability. Asian Journal of Pharmaceutical Sciences. 2014;9(6):304-316. https://doi.org/10.1016/j.ajps.2014.05.005

49. Sun J, Wang F, Sui Y, et al. Effect of particle size on solubility, dissolution rate, and oral bioavailability: evaluation using coenzyme Q_{10} as naked nanocrystals. Int J Nanomedicine. 2012;7:5733-5744. https://doi.org/10.2147/IJN.S34365

50. Junghanns J-UAH, Müller RH. Nanocrystal technology, drug delivery and clinical applications. Int J Nanomedicine. 2008;3(3):295-309. https://doi.org/10.2147/ijn.s595

51. Williams HD, Trevaskis NL, Charman SA, et al. Strategies to address low drug solubility in discovery and development. Pharmacol Rev. 2013;65(1):315-499. https://doi.org/10.1124/pr.112.005660

52. Zhang Y, Chan HF, Leong KW. Advanced materials and processing for drug delivery: the past and the future. Adv Drug Deliv Rev. 2013;65(1):104-120. https://doi.org/10.1016/j.addr.2012.10.003

53. Bajpai SK, Kirar N. Swelling and drug release behavior of calcium alginate/poly (sodium acrylate) hydrogel beads. Designed Monomers and Polymers. 2015;19(1):89-98. https://doi.org/10.1080/15685551.2015.1092016

54. Bhasarkar J, Bal D. Kinetic investigation of a controlled drug delivery system based on alginate scaffold with embedded voids. J Appl Biomater Funct Mater. 2019;17(2):2280800018817462. https://doi.org/10.1177/2280800018817462

55. Wong BS, Teoh S-H, Kang L. Polycaprolactone scaffold as targeted drug delivery system and cell attachment scaffold for postsurgical care of limb salvage. Drug Deliv Transl Res. 2012;2(4):272-283. https://doi.org/10.1007/s13346-012-0096-9

56. Cader HK, Rance GA, Alexander MR, et al. Water-based 3D inkjet printing of an oral pharmaceutical dosage form. Int J Pharm. 2019;564:359-368. https://doi.org/10.1016/j.ijpharm.2019.04.026

57. Wang J, Goyanes A, Gaisford S, Basit AW. Stereolithographic (SLA) 3D printing of oral modified-release dosage forms. Int J Pharm. 2016;503(1-2):207-212. https://doi.org/10.1016/j.ijpharm.2016.03.016

58. Khaled SA, Burley JC, Alexander MR, Yang J, Roberts CJ. 3D printing of five-in-one dose combination polypill with defined immediate and sustained release profiles. J Control Release. 2015;217:308-314. https://doi.org/10.1016/j.jconrel.2015.09.028

59. Clark EA, Alexander MR, Irvine DJ, et al. 3D printing of tablets using inkjet with UV photoinitiation. Int J Pharm. 2017;529(1-2):523-530. https://doi.org/10.1016/j.ijpharm.2017.06.085

60. Fina F, Madla CM, Goyanes A, Zhang J, Gaisford S, Basit AW. Fabricating 3D printed orally disintegrating printlets using selective laser sintering. Int J Pharm. 2018;541(1-2):101-107. https://doi.org/10.1016/j.ijpharm.2018.02.015

61. Solanki NG, Tahsin M, Shah AV, Serajuddin ATM. Formulation of 3D Printed Tablet for Rapid Drug Release by Fused Deposition Modeling: Screening Polymers for Drug Release, Drug-Polymer Miscibility and Printability. J Pharm Sci. 2018;107(1):390-401. https://doi.org/10.1016/j.xphs.2017.10.021

62. Goyanes A, Robles Martinez P, Buanz A, Basit AW, Gaisford S. Effect of geometry on drug release from 3D printed tablets. Int J Pharm. 2015;494(2):657-663. https://doi.org/10.1016/j.ijpharm.2015.04.069

63. Sadia M, Arafat B, Ahmed W, Forbes RT, Alhnan MA. Channelled tablets: An innovative approach to accelerating drug release from 3D printed tablets. J Control Release. 2018;269:355-363. https://doi.org/10.1016/j.jconrel.2017.11.022

64. Wickström H, Palo M, Rijckaert K, et al. Improvement of dissolution rate of indomethacin by inkjet printing. Eur J Pharm Sci. 2015;75:91-100. https://doi.org/10.1016/j.ejps.2015.03.009

65. Pardeike J, Strohmeier DM, Schrödl N, et al. Nanosuspensions as advanced printing ink for accurate dosing of poorly soluble drugs in personalized medicines. Int J Pharm. 2011;420(1):93-100. https://doi.org/10.1016/j.ijpharm.2011.08.033

66. Cheow WS, Kiew TY, Hadinoto K. Combining inkjet printing and amorphous nanonization to prepare personalized dosage forms of poorly-soluble drugs. Eur J Pharm Biopharm. 2015;96:314-321. https://doi.org/10.1016/j.ejpb.2015.08.012

67. Rowe CW, Katstra WE, Palazzolo RD, Giritlioglu B, Teung P, Cima MJ. Multimechanism oral dosage forms fabricated by three dimensional printing™. Journal of Controlled Release. 2000;66(1):11-17. https://doi.org/10.1016/s0168-3659(99)00224-2

68. Khaled SA, Burley JC, Alexander MR, Roberts CJ. Desktop 3D printing of controlled release pharmaceutical bilayer tablets. Int J Pharm. 2014;461(1-2):105-111. https://doi.org/10.1016/j.ijpharm.2013.11.021

69. Jivraj I I, Martini LG, Thomson CM. An overview of the different excipients useful for the direct compression of tablets. Pharm Sci Technol Today. 2000;3(2):58-63. https://doi.org/10.1016/s1461-5347(99)00237-0

70. Sastry SV, Nyshadham JR, Fix JA. Recent technological advances in oral drug delivery - a review. Pharm Sci Technol Today. 2000;3(4):138-145. https://doi.org/10.1016/s1461-5347(00)00247-9

71. Khaled SA, Burley JC, Alexander MR, Yang J, Roberts CJ. 3D printing of tablets containing multiple drugs with defined release profiles. Int J Pharm. 2015;494(2):643-650. https://doi.org/10.1016/j.ijpharm.2015.07.067

72. Ilyés K, Kovács NK, Balogh A, et al. The applicability of pharmaceutical polymeric blends for the fused deposition modelling (FDM) 3D technique: Material considerations-printability-process modulation, with consecutive effects on in vitro release, stability and degradation. Eur J Pharm Sci. 2019;129:110-123. https://doi.org/10.1016/j.ejps.2018.12.019

73. Matijašić G, Gretić M, Kezerić K, Petanjek J, Vukelić E. Preparation of Filaments and the 3D Printing of Dronedarone HCl Tablets for Treating Cardiac Arrhythmias. AAPS PharmSciTech. 2019;20(8):310. https://doi.org/10.1208/s12249-019-1522-9

74. Fina F, Goyanes A, Rowland M, Gaisford S, W Basit A. 3D Printing of Tunable Zero-Order Release Printlets. Polymers (Basel). 2020;12(8):1769. https://doi.org/10.3390/polym12081769

75. Saviano M, Aquino RP, Del Gaudio P, Sansone F, Russo P. Poly(vinyl alcohol) 3D printed tablets: The effect of polymer particle size on drug loading and process efficiency. Int J Pharm. 2019;561:1-8. https://doi.org/10.1016/j.ijpharm.2019.02.025

76. Li Q, Wen H, Jia D, et al. Preparation and investigation of controlled-release glipizide novel oral device with three-dimensional printing. Int J Pharm. 2017;525(1):5-11. https://doi.org/10.1016/j.ijpharm.2017.03.066

77. Linares V, Casas M, Caraballo I. Printfills: 3D printed systems combining fused deposition modeling and injection volume filling. Application to colon-specific drug delivery. Eur J Pharm Biopharm. 2019;134:138-143. https://doi.org/10.1016/j.ejpb.2018.11.021

78. Clark EA, Alexander MR, Irvine DJ, et al. Making tablets for delivery of poorly soluble drugs using photoinitiated 3D inkjet printing. Int J Pharm. 2020;578:118805. https://doi.org/10.1016/j.ijpharm.2019.118805

79. Kempin W, Domsta V, Grathoff G, et al. Immediate Release 3D-Printed Tablets Produced Via Fused Deposition Modeling of a Thermo-Sensitive Drug. Pharm Res. 2018;35(6):124. https://doi.org/10.1007/s11095-018-2405-6

80. Kollamaram G, Croker DM, Walker GM, Goyanes A, Basit AW, Gaisford S. Low temperature fused deposition modeling (FDM) 3D printing of thermolabile drugs. Int J Pharm. 2018;545(1-2):144-152. https://doi.org/10.1016/j.ijpharm.2018.04.055

81. Jamróz W, Kurek M, Szafraniec-Szczęsny J, et al. Speed it up, slow it down…An issue of bicalutamide release from 3D printed tablets. Eur J Pharm Sci. 2020;143:105169. https://doi.org/10.1016/j.ejps.2019.105169

82. Luongo F, Mangano FG, Macchi A, Luongo G, Mangano C. Custom-Made Synthetic Scaffolds for Bone Reconstruction: A Retrospective, Multicenter Clinical Study on 15 Patients. Biomed Res Int. 2016;2016:5862586. https://doi.org/10.1155/2016/5862586

83. Varan C, Wickström H, Sandler N, Aktaş Y, Bilensoy E. Inkjet printing of antiviral PCL nanoparticles and anticancer cyclodextrin inclusion complexes on bioadhesive film for cervical administration. Int J Pharm. 2017;531(2):701-713. https://doi.org/10.1016/j.ijpharm.2017.04.036

84. Muwaffak Z, Goyanes A, Clark V, Basit AW, Hilton ST, Gaisford S. Patient-specific 3D scanned and 3D printed antimicrobial polycaprolactone wound dressings. Int J Pharm. 2017;527(1-2):161-170. https://doi.org/10.1016/j.ijpharm.2017.04.077

85. Fu J, Yu X, Jin Y. 3D printing of vaginal rings with personalized shapes for controlled release of progesterone. Int J Pharm. 2018;539(1-2):75-82. https://doi.org/10.1016/j.ijpharm.2018.01.036

86. Goyanes A, Det-Amornrat U, Wang J, Basit AW, Gaisford S. 3D scanning and 3D printing as innovative technologies for fabricating personalized topical drug delivery systems. J Control Release. 2016;234:41-48. https://doi.org/10.1016/j.jconrel.2016.05.034

87. Lee K-J, Kang A, Delfino JJ, et al. Evaluation of critical formulation factors in the development of a rapidly dispersing captopril oral dosage form. Drug Dev Ind Pharm. 2003;29(9):967-979. https://doi.org/10.1081/ddc-120025454

88. Pere CPP, Economidou SN, Lall G, et al. 3D printed microneedles for insulin skin delivery. Int J Pharm. 2018;544(2):425-432. https://doi.org/10.1016/j.ijpharm.2018.03.031

89. Algahtani MS, Mohammed AA, Ahmad J, Saleh E. Development of a 3D Printed Coating Shell to Control the Drug Release of Encapsulated Immediate-Release Tablets. Polymers (Basel). 2020;12(6):1395. https://doi.org/10.3390/polym12061395

90. Pereira T, Kennedy JV, Potgieter J. A comparison of traditional manufacturing vs additive manufacturing, the best method for the job. Procedia Manufacturing. 2019;30:11-18. https://doi.org/10.1016/j.promfg.2019.02.003

91. Park JY, Kim HY, Kim JH, Kim JH, Kim WC. Comparison of prosthetic models produced by traditional and additive manufacturing methods. J Adv Prosthodont. 2015;7(4):294-302. https://doi.org/10.4047/jap.2015.7.4.294

92. Sinha SK. Additive manufacturing (AM) of medical devices and scaffolds for tissue engineering based on 3D and 4D printing. 3D and 4D Printing of Polymer Nanocomposite Materials, Elsevier; 2020. p. 119-160. https://doi.org/10.1016/b978-0-12-816805-9.00005-3

93. Beretta S, Romano S. A comparison of fatigue strength sensitivity to defects for materials manufactured by AM or traditional processes. International Journal of Fatigue. 2017;94:178-191. https://doi.org/10.1016/j.ijfatigue.2016.06.020

94. Goyanes A, Buanz ABM, Hatton GB, Gaisford S, Basit AW. 3D printing of modified-release aminosalicylate (4-ASA and 5-ASA) tablets. Eur J Pharm Biopharm. 2015;89:157-162. https://doi.org/10.1016/j.ejpb.2014.12.003

95. Yi H-G, Choi Y-J, Kang KS, et al. A 3D-printed local drug delivery patch for pancreatic cancer growth suppression. J Control Release. 2016;238:231-241. https://doi.org/10.1016/j.jconrel.2016.06.015

96. Karakurt I, Aydoğdu A, Çıkrıkcı S, Orozco J, Lin L. Stereolithography (SLA) 3D printing of ascorbic acid loaded hydrogels: A controlled release study. Int J Pharm. 2020;584:119428. https://doi.org/10.1016/j.ijpharm.2020.119428

97. Healy AV, Fuenmayor E, Doran P, Geever LM, Higginbotham CL, Lyons JG. Additive Manufacturing of Personalized Pharmaceutical Dosage Forms via Stereolithography. Pharmaceutics. 2019;11(12):645. https://doi.org/10.3390/pharmaceutics11120645

98. Goyanes A, Chang H, Sedough D, et al. Fabrication of controlled-release budesonide tablets via desktop (FDM) 3D printing. Int J Pharm. 2015;496(2):414-420. https://doi.org/10.1016/j.ijpharm.2015.10.039

99. Tagami T, Nagata N, Hayashi N, et al. Defined drug release from 3D-printed composite tablets consisting of drug-loaded polyvinylalcohol and a water-soluble or water-insoluble polymer filler. Int J Pharm. 2018;543(1-2):361-367. https://doi.org/10.1016/j.ijpharm.2018.03.057

100. Lim SH, Chia SMY, Kang L, Yap KY-L. Three-Dimensional Printing of Carbamazepine Sustained-Release Scaffold. J Pharm Sci. 2016;105(7):2155-2163. https://doi.org/10.1016/j.xphs.2016.04.031

101. Tagami T, Yoshimura N, Goto E, Noda T, Ozeki T. Fabrication of Muco-Adhesive Oral Films by the 3D Printing of Hydroxypropyl Methylcellulose-Based Catechin-Loaded Formulations. Biol Pharm Bull. 2019;42(11):1898-1905. https://doi.org/10.1248/bpb.b19-00481

102. Tagami T, Fukushige K, Ogawa E, Hayashi N, Ozeki T. 3D Printing Factors Important for the Fabrication of Polyvinylalcohol Filament-Based Tablets. Biol Pharm Bull. 2017;40(3):357-364. https://doi.org/10.1248/bpb.b16-00878

103. Beck RCR, Chaves PS, Goyanes A, et al. 3D printed tablets loaded with polymeric nanocapsules: An innovative approach to produce customized drug delivery systems. Int J Pharm. 2017;528(1-2):268-279. https://doi.org/10.1016/j.ijpharm.2017.05.074

104. Costa PF, Puga AM, Díaz-Gomez L, Concheiro A, Busch DH, Alvarez-Lorenzo C. Additive manufacturing of scaffolds with dexamethasone controlled release for enhanced bone regeneration. Int J Pharm. 2015;496(2):541-550. https://doi.org/10.1016/j.ijpharm.2015.10.055

105. Rattanakit P, Moulton SE, Santiago KS, Liawruangrath S, Wallace GG. Extrusion printed polymer structures: a facile and versatile approach to tailored drug delivery platforms. Int J Pharm. 2012;422(1-2):254-263. https://doi.org/10.1016/j.ijpharm.2011.11.007

106. Li Q, Guan X, Cui M, et al. Preparation and investigation of novel gastro-floating tablets with 3D extrusion-based printing. Int J Pharm. 2018;535(1-2):325-332. https://doi.org/10.1016/j.ijpharm.2017.10.037

107. Tagami T, Ito E, Hayashi N, Sakai N, Ozeki T. Application of 3D printing technology for generating hollow-type suppository shells. Int J Pharm. 2020;589:119825. https://doi.org/10.1016/j.ijpharm.2020.119825

108. Siyawamwaya M, du Toit LC, Kumar P, Choonara YE, Kondiah PPPD, Pillay V. 3D printed, controlled release, tritherapeutic tablet matrix for advanced anti-HIV-1 drug delivery. Eur J Pharm Biopharm. 2019;138:99-110. https://doi.org/10.1016/j.ejpb.2018.04.007

109. Kyobula M, Adedeji A, Alexander MR, et al. 3D inkjet printing of tablets exploiting bespoke complex geometries for controlled and tuneable drug release. J Control Release. 2017;261:207-215. https://doi.org/10.1016/j.jconrel.2017.06.025

110. Kao CT, Chen YJ, Huang TH, Lin YH, Hsu TT, Ho CC. Assessment of the Release Profile of Fibroblast Growth Factor-2-Load Mesoporous Calcium Silicate/ Poly-ε-caprolactone 3D Scaffold for Regulate Bone Regeneration. Processes. 2020;8(10):1249. https://doi.org/10.3390/pr8101249

111. Goyanes A, Buanz ABM, Basit AW, Gaisford S. Fused-filament 3D printing (3DP) for fabrication of tablets. Int J Pharm. 2014;476(1-2):88-92. https://doi.org/10.1016/j.ijpharm.2014.09.044

112. Weisman JA, Ballard DH, Jammalamadaka U, et al. 3D Printed Antibiotic and Chemotherapeutic Eluting Catheters for Potential Use in Interventional Radiology: In Vitro Proof of Concept Study. Acad Radiol. 2019;26(2):270-274. https://doi.org/10.1016/j.acra.2018.03.022

113. Wen H, He B, Wang H, et al. Structure-Based Gastro-Retentive and Controlled-Release Drug Delivery with Novel 3D Printing. AAPS PharmSciTech. 2019;20(2):68. https://doi.org/10.1208/s12249-018-1237-3

114. Gioumouxouzis CI, Baklavaridis A, Katsamenis OL, et al. A 3D printed bilayer oral solid dosage form combining metformin for prolonged and glimepiride for immediate drug delivery. Eur J Pharm Sci. 2018;120:40-52. https://doi.org/10.1016/j.ejps.2018.04.020

115. Martinez PR, Goyanes A, Basit AW, Gaisford S. Fabrication of drug-loaded hydrogels with stereolithographic 3D printing. Int J Pharm. 2017;532(1):313-317. https://doi.org/10.1016/j.ijpharm.2017.09.003

116. Ehtezazi T, Algellay M, Islam Y, Roberts M, Dempster NM, Sarker SD. The Application of 3D Printing in the Formulation of Multilayered Fast Dissolving Oral Films. J Pharm Sci. 2018;107(4):1076-1085. https://doi.org/10.1016/j.xphs.2017.11.019

117. Scoutaris N, Ross SA, Douroumis D. 3D Printed "Starmix" Drug Loaded Dosage Forms for Paediatric Applications. Pharm Res. 2018;35(2):34. https://doi.org/10.1007/s11095-017-2284-2

118. Holländer J, Genina N, Jukarainen H, et al. Three-Dimensional Printed PCL-Based Implantable Prototypes of Medical Devices for Controlled Drug Delivery. J Pharm Sci. 2016;105(9):2665-2676. https://doi.org/10.1016/j.xphs.2015.12.012

119. Genina N, Holländer J, Jukarainen H, Mäkilä E, Salonen J, Sandler N. Ethylene vinyl acetate (EVA) as a new drug carrier for 3D printed medical drug delivery devices. Eur J Pharm Sci. 2016;90:53-63. https://doi.org/10.1016/j.ejps.2015.11.005

120. Genina N, Boetker JP, Colombo S, Harmankaya N, Rantanen J, Bohr A. Anti-tuberculosis drug combination for controlled oral delivery using 3D printed compartmental dosage forms: From drug product design to in vivo testing. J Control Release. 2017;268:40-48. https://doi.org/10.1016/j.jconrel.2017.10.003

121. Smith D, Kapoor Y, Hermans A, et al. 3D printed capsules for quantitative regional absorption studies in the GI tract. Int J Pharm. 2018;550(1-2):418-428. https://doi.org/10.1016/j.ijpharm.2018.08.055

122. Huang W, Zheng Q, Sun W, Xu H, Yang X. Levofloxacin implants with predefined microstructure fabricated by three-dimensional printing technique. Int J Pharm. 2007;339(1-2):33-38. https://doi.org/10.1016/j.ijpharm.2007.02.021

123. García-Alvarez R, Izquierdo-Barba I, Vallet-Regí M. 3D scaffold with effective multidrug sequential release against bacteria biofilm. Acta Biomater. 2017;49:113-126. https://doi.org/10.1016/j.actbio.2016.11.028

124. Ibrahim M, Barnes M, McMillin R, et al. 3D Printing of Metformin HCl PVA Tablets by Fused Deposition Modeling: Drug Loading, Tablet Design, and Dissolution Studies. AAPS PharmSciTech. 2019;20(5):195. https://doi.org/10.1208/s12249-019-1400-5

125. Smith DM, Kapoor Y, Klinzing GR, Procopio AT. Pharmaceutical 3D printing: Design and qualification of a single step print and fill capsule. Int J Pharm. 2018;544(1):21-30. https://doi.org/10.1016/j.ijpharm.2018.03.056

126. Huanbutta K, Sangnim T. Design and development of zero-order drug release gastroretentive floating tablets fabricated by 3D printing technology. Journal of Drug Delivery Science and Technology. 2019;52:831-837. https://doi.org/10.1016/j.jddst.2019.06.004

127. Water JJ, Bohr A, Boetker J, et al. Three-dimensional printing of drug-eluting implants: preparation of an antimicrobial polylactide feedstock material. J Pharm Sci. 2015;104(3):1099-1107. https://doi.org/10.1002/jps.24305

128. Gbureck U, Vorndran E, Müller FA, Barralet JE. Low temperature direct 3D printed bioceramics and biocomposites as drug release matrices. J Control Release. 2007;122(2):173-180. https://doi.org/10.1016/j.jconrel.2007.06.022

129. Zhang J, Yang W, Vo AQ, et al. Hydroxypropyl methylcellulose-based controlled release dosage by melt extrusion and 3D printing: Structure and drug release correlation. Carbohydr Polym. 2017;177:49-57. https://doi.org/10.1016/j.carbpol.2017.08.058

130. Zhang J, Feng X, Patil H, Tiwari RV, Repka MA. Coupling 3D printing with hot-melt extrusion to produce controlled-release tablets. Int J Pharm. 2017;519(1-2):186-197. https://doi.org/10.1016/j.ijpharm.2016.12.049

131. Goyanes A, Fina F, Martorana A, Sedough D, Gaisford S, Basit AW. Development of modified release 3D printed tablets (printlets) with pharmaceutical excipients using additive manufacturing. Int J Pharm. 2017;527(1-2):21-30. https://doi.org/10.1016/j.ijpharm.2017.05.021

132. Fina F, Goyanes A, Gaisford S, Basit AW. Selective laser sintering (SLS) 3D printing of medicines. Int J Pharm. 2017;529(1-2):285-293. https://doi.org/10.1016/j.ijpharm.2017.06.082

133. Holländer J, Hakala R, Suominen J, Moritz N, Yliruusi J, Sandler N. 3D printed UV light cured polydimethylsiloxane devices for drug delivery. Int J Pharm. 2018;544(2):433-442. https://doi.org/10.1016/j.ijpharm.2017.11.016

134. Long J, Nand AV, Ray S, et al. Development of customised 3D printed biodegradable projectile for administrating extended-release contraceptive to wildlife. Int J Pharm. 2018;548(1):349-356. https://doi.org/10.1016/j.ijpharm.2018.07.002

135. Vakili H, Nyman JO, Genina N, Preis M, Sandler N. Application of a colorimetric technique in quality control for printed pediatric orodispersible drug delivery systems containing propranolol hydrochloride. Int J Pharm. 2016;511(1):606-618. https://doi.org/10.1016/j.ijpharm.2016.07.032

136. Genina N, Janßen EM, Breitenbach A, Breitkreutz J, Sandler N. Evaluation of different substrates for inkjet printing of rasagiline mesylate. Eur J Pharm Biopharm. 2013;85(3 Pt B):1075-1083. https://doi.org/10.1016/j.ejpb.2013.03.017

137. Wu G, Huang F, Huang Y, et al. Bone inductivity comparison of control versus non-control released rhBMP2 coatings in 3D printed hydroxyapatite scaffold. J Biomater Appl. 2020;34(9):1254-1266. https://doi.org/10.1177/0885328220903962

138. Fu J, Yin H, Yu X, et al. Combination of 3D printing technologies and compressed tablets for preparation of riboflavin floating tablet-in-device (TiD) systems. Int J Pharm. 2018;549(1-2):370-379. https://doi.org/10.1016/j.ijpharm.2018.08.011

139. Bom S, Santos C, Barros R, et al. Effects of Starch Incorporation on the Physicochemical Properties and Release Kinetics of Alginate-Based 3D Hydrogel Patches for Topical Delivery. Pharmaceutics. 2020;12(8):719. https://doi.org/10.3390/pharmaceutics12080719

140. Cheng Y, Qin H, Acevedo NC, Jiang X, Shi X. 3D printing of extended-release tablets of theophylline using hydroxypropyl methylcellulose (HPMC) hydrogels. Int J Pharm. 2020;591:119983. https://doi.org/10.1016/j.ijpharm.2020.119983

141. Sergeeva NS, Sviridova IK, Komlev VS, et al. 3D printed constructs with antibacterial or antitumor activity for surgical treatment of bone defects in cancer patients. AIP Conference Proceedings. AIP Publishing LLC; 2017, p. 020063. https://doi.org/10.1063/1.5001642

142. Arafat B, Qinna N, Cieszynska M, Forbes RT, Alhnan MA. Tailored on demand anti-coagulant dosing: An in vitro and in vivo evaluation of 3D printed purpose-designed oral dosage forms. Eur J Pharm Biopharm. 2018;128:282-289. https://doi.org/10.1016/j.ejpb.2018.04.010